389604-10-T

SCATTERING FROM TAPERED RESISTIVE SHEET JUNCTIONS

Leo C. Kempel
John L. Volakis
Thomas B.A. Senior

Northrop Corporation
8900 E. Washington Blvd.
Pico Rivera CA 90660-3737

September 1991

389604-10-T = RL-2569

Scattering from Tapered Resistive Sheet Junctions

Leo C. Kempel, John L. Volakis, and Thomas B.A. Senior

September 1991

Abstract

The scattering by the junction formed by two coplanar uniform impedance, resistive, or dielectric half planes has been considered in the past. In this report, we investigate the scattering by the junction formed by two tapered resistive sheets. In particular, the exact E-polarization diffraction coefficient for the junction of two coplanar linearly tapered resistive sheets is found by application of the Kontorovich-Lebedev transformation. In addition, a Physical Optics diffraction coefficient for the junction formed by a metallic half plane and a linearly or quadratically tapered resistive sheet for either E- or H-polarization is presented. All diffraction coefficients are compared to numerical results and the utility of each method is discussed.

Contents

1 Introduction

Although the scattering from various material half planes in isolation have been studied for over thirty years, the diffraction coefficient associated with the junction of two coplanar material half planes is a more recent development. Rojas[1] employed the Wiener-Hopf technique to determine the diffraction coefficient by two coplanar abutting impedance half planes. Ricoy and Volakis[2] utilized Generalized Impedance Boundary Conditions to study the diffraction from a dielectric join for normal incidence and Büyükaksoy *et al.*[3] used the Wiener-Hopf technique to determine the diffraction of an obliquely incident plane wave from the junction of two thin dielectrics. Büyükaksoy *et al.*[4] also examined the diffraction by the junction formed by an impedance and a resistive half plane. Senior[5] employed the angular spectrum method to determine the diffraction coefficient for any combination of coplanar abutting impedance, resistive, or conductive half planes. He showed that the resulting coefficient can be written as a product of the corresponding half plane diffraction coefficients in isolation. Furthermore, Senior[6] treated this case for skew incidence once again with the angular spectrum method.

All preceding analyses dealt with junctions having homogeneous electrical properties in either half plane. An exception is a solution presented by Yang *et al.*[7] for the scattering by a resistive sheet whose resistivity linearly increased from the origin. To do so, Yang *et al.*[7] solved the Helmholtz equation with the aid of the Kontorovich and Lebedev transform[8], hereafter referred to as the K-L transform.

This report is concerned with the investigation of the scattering by the junction formed by two sheets whose resistivity smoothly increases with distance from the junction. The E-polarization diffraction from the junction of two linearly tapered resistive sheets will be found by an extension of the method employed by Yang *et al.*[7]. This solution is verified by comparison with results based on numerical simulations employing the method of moments. We also consider a Physical Optics (PO) approximation of the E- and H-polarization scattering from the junction formed by a metallic and a tapered resistive half plane. The slope of the taper is, of course, important in assessing the validity limits of the PO approximation and this is examined by comparison with numerical data.

2 Diffraction by a Linearly,Tapered Resistive Sheet Junction

2.1 Formulation

Consider the case of two abutting coplanar resistive half planes in the $y = 0$ plane illustrated in figure 1a. We are interested in determining the diffracted field by the junction of these half planes when illuminated by the E-polarized plane wave

$$\vec{E}^i = \hat{z}e^{-ik\rho\cos(\phi-\phi_o)} \tag{1}$$

(an $e^{-i\omega t}$ time-dependence is assumed and suppressed) where k is the wavenumber, (ρ, ϕ) denote the normal cylindrical coordinates and ϕ_o is recognized as the angle of incidence. Each of the resistive sheets forming the junction has a linearly varying resistivity and satisfies the boundary conditions

$$\left[\hat{y} \times \vec{E}\right]_{y=0^-}^{y=0^+} = 0 \tag{2}$$

$$\hat{y} \times \left(\hat{y} \times \vec{E}\right) = -R(x)\left[\hat{y} \times \vec{H}\right]_{y=0^-}^{y=0^+} \tag{3}$$

where $[\ ]_{y=0^-}^{y=0^+}$ denotes the discontinuity in the value of the quantity above and below the sheet. Also,

$$\begin{aligned} R(x) &= R_1(x) = -a_1\frac{Z_o}{2}kx \quad x \le 0 \\ &= R_2(x) = +a_2\frac{Z_o}{2}kx \quad x \ge 0 \end{aligned} \tag{4}$$

is the resistivity profile of the half planes with Z_o being the free-space intrinsic impedance as illustrated in figure 1b. In (2) and (3), $\vec{E}$ and $\vec{H}$ denote total field quantities and for E-polarization the corresponding total and scattered electric fields will also be z-directed with the last defined as

$$E_z^s(\xi, \phi) = E_z(\xi, \phi) - E_z^i(\xi, \phi) \tag{5}$$

The scattered field satisfies the scalar Helmholtz equation

$$\left[\frac{\partial^2}{\partial\xi^2} + \frac{1}{\xi}\frac{\partial}{\partial\xi} + \frac{1}{\xi^2}\frac{\partial^2}{\partial\phi^2} + 1\right] E_z^s(\xi, \phi) = 0 \tag{6}$$

where $\xi = k\rho$, and to find $E_z^s(\xi, \phi)$ we must solve this equation subject to the radiation and the boundary conditions (2) and (3). To do so, we first note that

the boundary conditions are specified on the $\phi = 0$ and $\phi = \pi$ half planes and thus for a solution of (6), it is instructive to eliminate the ρ variable through a convenient transformation. The K-L transform is suitable for our case since it will be seen to completely eliminate the ρ dependence from the Helmholtz equation and boundary conditions for the resistivity profile given in (4). For our purposes, we denote the K-L transform pair as

$$F(\nu,\phi) = \int_0^\infty \frac{f(\xi,\phi)}{\xi} H_\nu^{(1)}(\xi)d\xi \tag{7}$$

$$f(\xi,\phi) = \frac{1}{i4}\int_{-i\infty}^{i\infty} \nu F(\nu,\phi)e^{i\nu\pi}\sin(\nu\pi)H_\nu^{(1)}(\xi)d\nu \tag{8}$$

and require the conditions $\lim_{\xi\to 0} f(\xi,\phi) = 0$ and $Im[k] > 0$ be satisfied to ensure convergence of the integrals. To satisfy the requirement on $f(\xi,\phi)$ as $\xi \to 0$, we set

$$E_z^s(\xi,\phi) + f_o e^{i\xi} = f(\xi,\phi) \tag{9}$$

where $f_o = E^s(\rho = 0,\phi)$ and in accordance with the edge condition $\lim_{\rho\to 0}(\rho H_\rho) = 0$ it follows that $f_o = +1$.

In view of (9), (6) can now be rewritten as

$$\left[\xi^2\frac{\partial^2}{\partial\xi^2} + \xi\frac{\partial}{\partial\xi} + \frac{\partial^2}{\partial\phi^2} + \xi^2\right] f(\xi,\phi) = i\xi e^{i\xi} \tag{10}$$

and upon taking the K-L transform of both sides of this equation we obtain

$$\begin{aligned}\left[\frac{\partial^2}{\partial\phi^2} + \nu^2\right] F(\nu,\phi) &= i\int_0^\infty e^{i\xi}H_\nu^{(1)}(\xi)d\xi \\ &= i2\frac{\nu e^{-i\nu\frac{\pi}{2}}}{\sin(\pi\nu)}\end{aligned} \tag{11}$$

This is a second-order differential equation in ϕ and can be readily solved in terms of the transform variable ν. We have

$$\begin{aligned}F(\nu,\phi) &= i2\frac{e^{-i\nu\frac{\pi}{2}}}{\nu\sin(\pi\nu)} + A\cos(\phi\nu) + B\sin(\phi\nu) \quad 0 \le \phi < \pi \\ &= i2\frac{e^{-i\nu\frac{\pi}{2}}}{\nu\sin(\pi\nu)} + C\cos(\phi\nu) + D\sin(\phi\nu) \quad \pi < \phi \le 2\pi\end{aligned} \tag{12}$$

with the constants A,B,C and D to be determined from the boundary conditions on either side of the junction. For this purpose it is convenient to first rewrite the

boundary conditions (2) and (3) as

$$E_z(\xi,\pi^+) = E_z(\xi,\pi^-) \tag{13}$$

$$E_z(\xi,\pi^+) = i\frac{Y_o R_1(\xi)}{\xi}\left[\frac{\partial E_z}{\partial\phi}(\xi,\phi)\right]_{\phi=\pi^-}^{\phi=\pi^+} \tag{14}$$

$$E_z(\xi,0) = E_z(\xi,2\pi) \tag{15}$$

$$E_z(\xi,0) = -i\frac{Y_o R_2(\xi)}{\xi}\left[\frac{\partial E_z}{\partial\phi}(\xi,\phi)\right]_{\phi=2\pi}^{\phi=0} \tag{16}$$

where $R_{1,2}(\xi)$ denote the arbitrary resistivity function for the left and right half planes. Specializing $R_{1,2}(\xi)$ to the case of a linear taper as given in (4) and making use of (1), (5) and (9) yields

$$f(\xi,\pi^+) = f(\xi,\pi^-) \tag{17}$$

$$f(\xi,\pi^+) = i\frac{a_1}{2}\left[\frac{\partial f}{\partial\phi}(\xi,\phi)\right]_{\phi=\pi^-}^{\phi=\pi^+} - \left(e^{i\xi\cos\phi_o} - e^{i\xi}\right) \tag{18}$$

$$f(\xi,0) = f(\xi,2\pi) \tag{19}$$

$$f(\xi,0) = -i\frac{a_2}{2}\left[\frac{\partial f}{\partial\phi}(\xi,\phi)\right]_{\phi=2\pi}^{\phi=0} - \left(e^{-i\xi\cos\phi_o} - e^{i\xi}\right) \tag{20}$$

and upon taking their K-L transforms, we obtain

$$F(\nu,\pi^+) = F(\nu,\pi^-) \tag{21}$$

$$F(\nu,\pi^+) = i\frac{a_1}{2}\left[\frac{\partial F}{\partial\phi}(\nu,\phi)\right]_{\phi=\pi^-}^{\phi=\pi^+} + i2\frac{e^{-i\nu\frac{\pi}{2}}}{\nu\sin(\pi\nu)}(1-\cos(\phi_o\nu)) \tag{22}$$

$$F(\nu,0) = F(\nu,2\pi) \tag{23}$$

$$F(\nu,0) = -i\frac{a_2}{2}\left[\frac{\partial F}{\partial\phi}(\nu,\phi)\right]_{\phi=2\pi}^{\phi=0} + i2\frac{e^{-i\nu\frac{\pi}{2}}}{\nu\sin(\pi\nu)}(1-\cos[(\pi-\phi_o)\nu]) \tag{24}$$

which are compatible with the differential equation (11).

Application of (21) and (23) to (12) allows the elimination of two of the unknown constants giving

$$\begin{aligned} F(\nu,\phi) &= i2\frac{e^{-i\nu\frac{\pi}{2}}}{\nu\sin(\pi\nu)} + C\cos[(2\pi-\phi)\nu] + D\sin[(2\pi-\phi)\nu] \quad 0\le\phi<\pi \\ &= i2\frac{e^{-i\nu\frac{\pi}{2}}}{\nu\sin(\pi\nu)} + C\cos(\phi\nu) + D\sin(\phi\nu) \quad \pi<\phi\le 2\pi \end{aligned} \tag{25}$$

The remaining constants may be determined by enforcing (22) and (24) and in doing so we obtain the solution

$$\begin{aligned} F(\nu,\phi) &= i2\frac{e^{-i\nu\frac{\pi}{2}}}{\nu\sin(\pi\nu)}\left[1-\frac{1}{\Gamma}\left\{\cos\left[(\pi-\phi-\phi_o)\nu\right]\right.\right. \\ &\quad +ia_1\nu\frac{\cos\left[(\pi-\phi)\nu\right]\cos\left[(\pi-\phi_o)\nu\right]}{\sin(\pi\nu)} \\ &\quad \left.\left.+ia_2\nu\frac{\cos(\phi\nu)\cos(\phi_o\nu)}{\sin(\pi\nu)}\right\}\right] \quad 0\le\phi<\pi \\ &= i2\frac{e^{-i\nu\frac{\pi}{2}}}{\nu\sin(\pi\nu)}\left[1-\frac{1}{\Gamma}\left\{\cos\left[(\pi-\phi-\phi_o)\nu\right]\right.\right. \\ &\quad +ia_1\nu\frac{\cos\left[(\phi-\pi)\nu\right]\cos\left[(\pi-\phi_o)\nu\right]}{\sin(\pi\nu)} \\ &\quad \left.\left.+ia_2\nu\frac{\cos\left[(2\pi-\phi)\nu\right]\cos(\phi_o\nu)}{\sin(\pi\nu)}\right\}\right] \quad \pi<\phi\le 2\pi \end{aligned} \tag{26}$$

where $\Gamma = 1 + a_1a_2\nu^2 + i(a_1+a_2)\nu\cot(\pi\nu)$. We observe that the form of $F(\nu,\phi)$ in the region $\pi < \phi \le 2\pi$ differs from that in $0 \le \phi < \pi$ by having $2\pi - \phi$ in place of ϕ and therefore it is sufficient to confine our attention to the case where $0 \le \phi < \pi$.

From (7) and (9), we can express the K-L transform of the scattered field as

$$\begin{aligned} E_z^s(\nu,\phi) &= F(\nu,\phi) - \int_0^\infty \frac{e^{i\xi}}{\xi}H_\nu^{(1)}d\xi \\ &= F(\nu,\phi) - i2\frac{e^{-i\nu\frac{\pi}{2}}}{\nu\sin(\pi\nu)} \end{aligned} \tag{27}$$

and upon taking the inverse transform of this, we have

$$\begin{aligned} E_z^s(\rho,\phi) &= -\frac{1}{2}\int_{-i\infty}^{i\infty}\frac{1}{\Gamma}\left\{\cos\left[(\pi-\phi-\phi_o)\nu\right]\right. \\ &\quad +ia_1\nu\frac{\cos\left[(\pi-\phi)\nu\right]\cos\left[(\pi-\phi_o)\nu\right]}{\sin(\pi\nu)} \\ &\quad \left.+ia_2\nu\frac{\cos(\phi\nu)\cos(\phi_o\nu)}{\sin(\pi\nu)}\right\}e^{i\nu\frac{\pi}{2}}H_\nu^{(1)}(k\rho)d\nu \end{aligned} \tag{28}$$

which is a complete representation of the scattered field. As a check, if we set $a_1 = a_2 = 0$, (28) gives

$$\begin{aligned} E_z^s(\rho,\phi) &= -\frac{1}{2}\int_{-i\infty}^{i\infty}\cos\left[(\pi-\phi-\phi_o)\right]e^{i\nu\frac{\pi}{2}}H_\nu^{(1)}(k\rho)d\nu \\ &= -e^{-ik\rho\cos(\phi+\phi_o)} \end{aligned} \tag{29}$$

which is the known reflected field from an infinite metallic plate.

Of primary interest in this study is the far-field. In this case $k\rho \to \infty$ and upon replacing the Hankel function in (28) with its large argument approximation, we find

$$E_z^s(\rho,\phi) \sim \sqrt{\frac{2}{\pi k\rho}} e^{i\left(k\rho-\frac{\pi}{4}\right)} D_e(\phi,\phi_o) \tag{30}$$

where

$$\begin{aligned} D_e(\phi,\phi_o) &= -\frac{1}{2}\int_{-i\infty}^{i\infty} \frac{1}{\Gamma}\Bigg\{ \cos\left[(\pi-\phi-\phi_o)\nu\right] \\ &\quad + ia_1\nu \frac{\cos\left[(\pi-\phi)\nu\right]\cos\left[(\pi-\phi_o)\nu\right]}{\sin(\pi\nu)} \\ &\quad + ia_2\nu \frac{\cos(\phi\nu)\cos(\phi_o\nu)}{\sin(\pi\nu)} \Bigg\} d\nu \end{aligned} \tag{31}$$

is the diffraction coefficient for the linearly tapered resistive sheet junction.

If we allow $a_1 \to \infty$ the left resistive sheet vanishes and the diffraction coefficient reduces to

$$D_e(\phi,\phi_o) = -\frac{1}{2}\int_{-i\infty}^{i\infty} \frac{\cos\left[(\pi-\phi)\nu\right]\cos\left[(\pi-\phi_o)\nu\right]}{\cos(\pi\nu) - ia_2\nu\sin(\pi\nu)} d\nu \tag{32}$$

which is the result derived by Yang *et al.*[7] for a half plane in isolation whose resistivity is linearly increasing away from the origin. Alternatively, if we set $a_2 = 0$ in (32), the resulting structure is a metallic half plane and as expected the associated diffraction coefficient is

$$\begin{aligned} D_e(\phi,\phi_o) &= -\frac{1}{2}\int_{-i\infty}^{i\infty} \frac{\cos\left[(\pi-\phi)\nu\right]\cos\left[(\pi-\phi_o)\nu\right]}{\cos(\pi\nu)} d\nu \\ &= -i\frac{\cos\left(\frac{\phi}{2}\right)\cos\left(\frac{\phi_o}{2}\right)}{\cos(\phi)+\cos(\phi_o)} \end{aligned} \tag{33}$$

Clearly the results in (32) and (33) serve as a partial validation of the solution(31).

2.2 Special case: Metallic-Linearly Tapered Resistive Half Plane Junction

As stated earlier, a particular case of interest is the diffraction by the junction formed by a metallic half plane and a resistive half plane whose resistivity is linearly increasing away from the junction. This corresponds to the case where $a_1 = 0$ and $a_2 \geq 0$ as shown in figure 1c and from (31) we obtain

$$D_e(\phi,\phi_o) = -\frac{1}{2}\int_{-i\infty}^{i\infty} \frac{\sin(\pi\nu)\cos\left[(\pi-\phi-\phi_o)\nu\right] + ia_2\nu\cos(\phi\nu)\cos(\phi_o\nu)}{\sin(\pi\nu)+ia_2\nu\cos(\pi\nu)}d\nu \quad (34)$$

For the remainder of this section, we shall concentrate on this type of a configuration. As a first step in evaluating the infinite integral of (34), we recognize that (34) may be alternatively written as

$$\begin{aligned} D_e(\phi,\phi_o) &= -\frac{1}{2}\int_{-i\infty}^{i\infty} \frac{\cos(\phi\nu)\cos(\phi_o\nu)}{cos(\pi\nu)}d\nu \\ &\quad +\frac{1}{2}\int_{-i\infty}^{i\infty} \frac{\tan(\pi\nu)\sin\left[(\pi-\phi)\nu\right]\sin\left[(\pi-\phi_o)\nu\right]}{\sin(\pi\nu)+ia_2\nu\cos(\pi\nu)}d\nu \end{aligned} \quad (35)$$

The first term in (35) is the diffraction coefficient for the metallic half plane and we can then infer that the second term is caused by the presence of the linearly tapered sheet. Consequently we can express (35) as

$$D_e(\phi,\phi_o) = D_e^{(1)}(\phi,\phi_o) + D_e^{(2)}(\phi,\phi_o) \quad (36)$$

where $D_e^{(1)}$ is given by (33) and

$$D_e^{(2)}(\phi,\phi_o) = \frac{1}{2}\int_{-i\infty}^{i\infty} \frac{\tan(\pi\nu)\sin\left[(\pi-\phi)\nu\right]\sin\left[(\pi-\phi_o)\nu\right]}{\sin(\pi\nu)+ia_2\nu\cos(\pi\nu)}d\nu \quad (37)$$

To evaluate the last integral, it is important to recognize that the integrand is even and its behavior as $\nu \to i\infty$ is

$$\lim_{\nu\to i\infty} \frac{\tan(\pi\nu)\sin\left[(\pi-\phi)\nu\right]\sin\left[(\pi-\phi_o)\nu\right]}{\sin(\pi\nu)+ia_2\nu\cos(\pi\nu)} = -\frac{1}{2(1+a_2\nu)}e^{i\nu(\phi-\pi+\phi_o)} \quad (38)$$

Adding and subtracting this result from the integrand of (37) we obtain

$$\begin{aligned} D_e^{(2)}(\phi,\phi_o) = & \quad -\tfrac{1}{2}\textstyle\int_0^{i\infty} \frac{e^{i\nu(\phi-\pi+\phi_o)}}{1+a_2\nu}d\nu \\ & +\textstyle\int_0^{i\infty} \left[\frac{\tan(\pi\nu)\sin[(\pi-\phi)\nu]\sin[(\pi-\phi_o)\nu]}{\sin(\pi\nu)+ia_2\nu\cos(\pi\nu)} + \frac{e^{i\nu(\phi-\pi+\phi_o)}}{2(1+a_2\nu)}\right]d\nu \end{aligned} \quad (39)$$

and it is recognized that the first integral is the tabulated exponential integral while the second term is a rapidly convergent integral which can be evaluated numerically. The diffraction coefficient for the metal-linearly tapered resistive junction can then be written as

$$D_e(\phi,\phi_o) = -i\frac{\cos\left(\frac{\phi}{2}\right)\cos\left(\frac{\phi_o}{2}\right)}{\cos(\phi)+\cos(\phi_o)} - \frac{1}{2a_2}e^{-\frac{i}{a_2}(\phi-\pi+\phi_o)}E_1\left[-\frac{i}{a_2}(\phi-\pi+\phi_o)\right] + \int_0^{i\infty}\left[\frac{\tan(\pi\nu)\sin[(\pi-\phi)\nu]\sin[(\pi-\phi_o)\nu]}{\sin(\pi\nu)+ia_2\nu\cos(\pi\nu)} + \frac{e^{i\nu(\phi-\pi+\phi_o)}}{2(1+a_2\nu)}\right]d\nu \tag{40}$$

where $E_1[\ ]$ denotes the exponential integral defined in Abramowitz and Stegun[9], and since the last integral is rapidly convergent, $D_e(\phi,\phi_o)$ can be readily evaluated from this expression.

3 Numerical Verification

In the preceding section we derived the diffraction coefficient for the junction formed by a metallic half plane and a resistive half plane having a resistivity which is linearly increasing away from the join. In this section we present a numerical validation of the analytical solution. The numerical simulation was achieved by truncating the resistive cards at a finite distance away from the junction and for the metallic half plane portion, a so-called killer-card was attached at the truncation point to suppress the diffraction from the end. The killer-card is essentially a finite size tapered resistive card and for effective suppression of the undesired edge diffracted field its resistivity is chosen to match that of the original half plane at the attachment point and is then tapered away from the truncation point. Initially this tapering provides a gradual increase in the resistivity of the card which becomes more rapid until the resistivity is very large.

After some experimentation, it was found that for E-polarization a suitable resistivity profile for simulating the metallic-linearly increasing resistive half plane junction is

$$\begin{aligned} R(x) &= 60.0Z_o\left[\frac{x+10.0}{30}\right]^{16} && -40 \le x \le -10 \\ &= 0.0 && -10 \le x \le 0 \\ &= a_2\pi Z_o x && 0 \le x \le x_{term} \end{aligned} \tag{41}$$

The first term of (41) is recognized as a 30λ killer-card and the second term is the truncated metallic half plane. If we allow $a_2 \to \infty$ in (41), a metallic half plane is simulated and the suitability of (41) in modeling the metallic half plane portion of the junction is demonstrated in figure 2 by comparison with the exact metallic half plane diffraction coefficient. The right half plane ($x \ge 0$), which has a linearly growing resistivity away from the junction, was truncated at the point where the current was approximately 10 percent of its average value over the length of the card. For example, figure 3a illustrates the resistivity profile(41) for $a_2 = 1$ where the right-side card was truncated at $x_{term} = 20\lambda$. The resulting computed current at edge-on incidence is illustrated in figure 3b and we observe that the termination criterion given previously is satisfied. Furthermore, it is interesting to point out that the current behavior near the junction, ($x = 0$), supports the observation made previously that the diffraction coefficient may be written as the sum of the metallic diffraction coefficient and a correction term.

Figures 4-13 compare the backscatter pattern of the diffraction coefficient(40) with corresponding numerical data for a variety of metallic half plane- linearly tapered resistive half plane junctions. Each figure corresponds to a different resistivity slope, πa_2, and as seen the derived diffraction coefficient agrees in all

cases with the numerical data. We observe that for large slopes, as expected, the diffraction coefficient approaches that of the metallic half plane. When $a_2 = 2$, the edge-on echowidth is about 10 dB below that of the metallic half plane and it is within a decibel of the metallic half plane echowidth when $a_2 = 10$. For $a_2 = 1$, the echowidth is down by 20 dB and for $a_2 = 0.5$ it is down by 30 dB. We remark that the numerical simulation of the smaller slope tapers is rather difficult since it requires x_{term} to be very large and the small discrepancies at edge-on in figures 4 and 5 are attributed to this problem.

4 PO Approximation for Metallic Half Plane-Tapered Sheet Junction

4.1 E-Polarization

Upon inspection of the boundary conditions for an E-polarized excitation it is clear from (13)-(16) that the analysis for the solution of the scalar wave equation in the K-L transform domain is useful only for the junction formed by two coplanar linearly tapered resistive half planes. However, it has been suggested by Haupt and Liepa[10] that the PO approximation is suitable for evaluating the scattering from slowly varying tapered sheets. Herein, we examine the accuracy of the PO approximation for the junction formed by a metallic half plane and a half plane whose resistivity increases either linearly or quadratically away from the junction.

The PO current due to an E-polarized plane wave excitation can be readily determined via the procedure followed by Haupt and Liepa[10]. Skipping the details, we obtain

$$\vec{J}^{PO}(x) = \hat{z}2Y_o \frac{\sin\phi_o}{1+2Y_o\sin\phi_o R(x)} e^{-ik_o\cos\phi_o x} \tag{42}$$

which is in agreement with the result of Haupt and Liepa[10]. The associated scattered field is then given by

$$\begin{aligned} \vec{E}^s &= \nabla\left(\nabla\cdot\vec{\Pi}^e\right) + k_o^2\vec{\Pi}^e \\ &= k^2\vec{\Pi}^e \\ &= -\hat{z}Z_o\frac{k}{4}\int_{-\infty}^{\infty} J_z\left(x'\right) H_o^{(1)}\left[k|x-x'|\right]dx' \end{aligned} \tag{43}$$

where $\frac{i}{4}H_o^{(1)}[k|x-x'|]$ is the two-dimensional free-space Green's function. To obtain the far-zone field, we introduce the large argument approximation for the Hankel function and this yields

$$\vec{E}^s \sim \hat{z}\sqrt{\frac{2}{\pi k_o\rho}} e^{i\left(k_o\rho-\frac{\pi}{4}\right)} P_e\left(\phi,\phi_o\right) \tag{44}$$

where the far-field coefficient is given by

$$P_e(\phi,\phi_o) = -Z_o\frac{k}{4}\int_{-\infty}^{\infty} J_z^{PO}\left(x'\right) e^{-ik\cos\phi x'} dx' \tag{45}$$

with $J_z^{PO}(x')$ as defined in (42).

To proceed with the evaluation of the integral in (45), we must first specify the resistivity profile function, R(x), which appears in (42). For the metallic half plane-linearly tapered half plane junction we have

$$\begin{aligned} R(x) &= 0 \qquad -\infty < x \leq 0 \\ &= Z_o a_2 \pi x \qquad 0 \leq x < \infty \end{aligned} \tag{46}$$

and when this is substituted in (42) and then in (45) we obtain the integral

$$\begin{aligned} I(\phi, \phi_o) &= \int_{-\infty}^{\infty} \frac{e^{-ik[\cos\phi + \cos\phi_o]x'}}{1 + 2Y_o \sin\phi_o R(x')} dx' \\ &= I_-(\phi, \phi_o) + I_+(\phi, \phi_o) \end{aligned} \tag{47}$$

The functions $I_\pm(\phi, \phi_o)$ are given by

$$\begin{aligned} I_-(\phi, \phi_o) &= \int_{-\infty}^{0} e^{-ik[\cos\phi + \cos\phi_o]x'} dx' \\ &= \pi\delta(\alpha) + \frac{i}{\alpha} \end{aligned} \tag{48}$$

and

$$\begin{aligned} I_+(\phi, \phi_o) &= \int_{0}^{\infty} \frac{e^{-ik[\cos\phi + \cos\phi_o]x'}}{1 + 2\pi a_2 \sin\phi_o x'} dx' \\ &= \beta e^{i\alpha\beta} E_1(i\alpha\beta) \end{aligned} \tag{49}$$

in which $\delta(x)$ denotes the impulse function, $\alpha = k[\cos\phi + \cos\phi_o]$, and $\beta = \frac{1}{2\pi a_2 \sin\phi_o}$. Consequently we may write $P_e(\phi, \phi_o)$

$$P_e(\phi, \phi_o) = -\frac{k_o}{4}\left[2\pi \sin\phi_o \delta(\alpha) + i2\frac{\sin\phi_o}{\alpha} + \frac{1}{\pi a_2} e^{i\alpha\beta} E_1(i\alpha\beta)\right] \tag{50}$$

which provides the far-field pattern due to the PO current and should be compared with the exact diffraction coefficient $D_e(\phi, \phi_o)$ given in the previous section

In figures 14-21, the far-field coefficient $P_e(\phi, \phi_o)$ is compared to the diffraction coefficient(40) for various slope parameters, a_2. For very gradual tapers ($a_2 \leq 0.2$), the PO approximation is seen to be in excellent agreement with the rigorous diffraction coefficient. However, for more rapidly increasing tapers, the PO approximation degrades, particularly at edge-on incidence. This is because the dominant scattering contribution away from broadside emanates from the discontinuity in the first derivative of the resistivity at the origin. Since this term is negligible for gradual tapers, PO works well for small a_2 and fails for the more rapid tapers.

If the dominant scattering is caused by discontinuities in the derivative of the resistivity profile, we then expect the PO approximation to perform better for a metal half plane joined to a quadratically tapered resistive half plane since the first derivative is continuous at the junction. Let us for example consider the following resistivity profile

$$\begin{aligned} R(x) &= 0 \qquad -\infty < x \leq 0 \\ &= Z_o b_2 \pi x^2 \qquad 0 \leq x < \infty \end{aligned} \tag{51}$$

Using the same procedure as before, we find that

$$\begin{aligned} P_e(\phi, \phi_o) &= -\frac{k_o}{2} \sin\phi_o \Big[\pi\delta(\alpha) + \frac{i}{\alpha} \\ &\quad + i\frac{\beta}{2}\left(e^{-\alpha\beta} E_i(\alpha\beta) + e^{\alpha\beta} E_1(\alpha\beta) + i\pi e^{-\alpha\beta} \right) \Big] \quad \alpha \geq 0 \\ &= -\frac{k_o}{2} \sin\phi_o \Big[\pi\delta(\alpha) + \frac{i}{\alpha} \\ &\quad - i\frac{\beta}{2}\left(e^{\alpha\beta} E_i(-\alpha\beta) + e^{-\alpha\beta} E_1(-\alpha\beta) + i\pi e^{\alpha\beta} \right) \Big] \quad \alpha \leq 0 \end{aligned} \tag{52}$$

where now $\beta = \frac{1}{\sqrt{2\pi b_2 \sin\phi_o}}$ and α is the same as before.

Figures 22-27 compare the above PO approximation to numerical data obtained by truncating the resistivity profile(51) and attaching a killer-card as done previously for the linearly varying sheet. Although it is difficult to numerically model gradual tapers due to computational size limitations and floating-point accuracy concerns, the numerical data indicates that the PO approximation is excellent up to $b_2 = 0.5$. For larger b_2, the PO approximation begins to fail for predictions near edge-on incidence. As seen from figures 26 and 27, the deviation from the numerical result which is our reference is quite substantial (more than 20dB) for $b_2 > 1$.

4.2 H-Polarization

Let us now consider the scattering by the tapered resistive sheet junction illuminated by the H-polarized plane wave

$$\vec{H}^i = \hat{z}e^{-jk\rho\cos(\phi-\phi_o)} \tag{53}$$

Unfortunately, for this illumination the analysis employed for E-polarization in the case of linearly tapered sheets is not applicable for H-polarization. To demonstrate this, let us examine the transition conditions for H-polarization. We have

$$\frac{\partial H_z}{\partial\phi}(\xi,\pi^+) = \frac{\partial H_z}{\partial\phi}(\xi,\pi^-) \tag{54}$$

$$\frac{\partial H_z}{\partial\phi}(\xi,\pi^+) = iY_o\xi R(x)\left[H_z(\xi,\phi)\right]_{\phi=\pi^-}^{\phi=\pi^+} \tag{55}$$

$$\frac{\partial H_z}{\partial\phi}(\xi,0) = \frac{\partial H_z}{\partial\phi}(\xi,2\pi) \tag{56}$$

$$\frac{\partial H_z}{\partial\phi}(\xi,0) = -iY_o\xi R(x)\left[H_z(\xi,\phi)\right]_{\phi=2\pi}^{\phi=0} \tag{57}$$

and it is obvious that the resistivity function which renders this condition independent of ξ is $R(x) = Z_o a_2/\xi$ which is not of practical interest. Thus, the K-L transform does not provide a direct means to solve for the H-polarization difraction from any useful taper.

At this point we are therefore forced to consider a PO approximation for the scattering by a junction formed by two tapered resistive half planes. We find that the PO current on a resistive plane is given by

$$\vec{J}(x) = \hat{x}\frac{2Y_o\sin\phi_o}{2Y_oR(x)+\sin\phi_o}e^{-ik\cos\phi_o x} \tag{58}$$

which agrees with the result given by Haupt [9]. Using this in the radiation integral we find that the far zone field is given by

$$\vec{E}^s \sim \hat{x}\sqrt{\frac{2}{\pi k\rho}}e^{i\left(k\rho-\frac{\pi}{4}\right)}P_h(\phi,\phi_o)$$

where

$$P_h(\phi,\phi_o) = Z_o\frac{k}{4}\sin\phi_o\int_{-\infty}^{\infty}J_x(x')e^{-ik_o\cos\phi x'}dx' \tag{59}$$

For the case of a junction formed by a metal half plane and a linearly tapered resistive sheet, the above integral can be evaluated in a manner similar to that

used for H-polarization to find

$$P_h(\phi,\phi_o) = \frac{k}{2}\sin\phi\left[\pi\delta(\alpha)+\frac{i}{\alpha}+\beta e^{i\alpha\beta}E_1(i\alpha\beta)\right] \tag{60}$$

where as before $\alpha = k(\cos\phi+\cos\phi_o)$ and $\beta = \frac{\sin\phi_o}{2\pi a_2}$. If $R(x)$ in (58) corresponds to a junction formed by a metal half plane and a quadratically tapered resistive sheet it follows that

$$\begin{aligned} P_h(\phi,\phi_o) &= \frac{k_o}{2}\sin\phi\Bigg[\pi\delta(\alpha)+\frac{i}{\alpha} \\ &\quad +i\frac{\beta}{2}\left(e^{-\alpha\beta}E_i(\alpha\beta)+e^{\alpha\beta}E_1(\alpha\beta)+i\pi e^{-\alpha\beta}\right)\Bigg] \quad \alpha\geq 0 \\ &= \frac{k_o}{2}\sin\phi\Bigg[\pi\delta(\alpha)+\frac{i}{\alpha} \\ &\quad -i\frac{\beta}{2}\left(e^{\alpha\beta}E_i(-\alpha\beta)+e^{-\alpha\beta}E_1(-\alpha\beta)+i\pi e^{\alpha\beta}\right)\Bigg] \quad \alpha\leq 0 \end{aligned} \tag{61}$$

where now $\beta = \sqrt{\frac{\sin\phi_o}{2\pi b_2}}$ and α is the same as before.

To examine the validity range of the PO approximation for H-polarization we again resorted to a numerical simulation of the corresponding junction. As in the case of E-polarization the metallic half plane is truncated at $x=-10\lambda$ at which point a killer-card is attached having the resistivity profile

$$R(x) = 20Z_o\left(\frac{x+10}{30}\right)^{16} \quad -40\lambda\leq x\leq -10\lambda \tag{62}$$

The linearly or quadratically tapered half plane is simply terminated at x_{term} where the current has dropped more than 90% of its average value over the range $0<x<x_{term}$. From the patterns shown in figure 28-31 it is seen that the PO approximation provides a reasonable simulation for $a_2\leq 0.7$ when the resistivity profile of the left half plane is linear. The inadequacy of the PO approximation is most apparent for incidences near grazing to the metallic half plane. However, it should be noted that the oscillatory behavior of the numerical result is characteristic to the numerical model (see Herrmann[11]) and not to the junction itself. The correct pattern is more likely to be the average line through the oscillations and the above statement on the validity of the PO approximation was based on this assumption.

Figures 32-35 include H-polarization patterns for the diffraction by a junction metal-resistive junction where the resistive half plane is now quadratically tapered away from the junction. From these figure it follows that the validity of the PO approximation is now extended up to $b_2\leq 2$. Again the failure of the PO approximation is more pronounced for incidences near grazing to the metallic half plane.

5 Summary and Conclusions

In this report we examined the diffraction by junctions formed by tapered resistive half planes. Particular emphasis was given to the case where the resistivity of the half planes grows linearly or quadratically away from the junction. For linear resistivities, rigorous analytical expressions were derived when the illumination was E-polarized, but unfortunately, we were not able to do the same for H-polarization. In the case of H-polarization we resorted to a PO approximation with emphasis on the metal-tapered resistive half plane junction. The accuracy of this PO approximation was examined by comparison with data from a numerical model where killer-cards were used to terminate the metallic half plane. It was found that the accuracy of the PO approximation for H-polarization is acceptable when the coefficient of the linear taper is less than 0.7 and in the quadratic tapers when the coefficient is less than 2. Essentially, by using a quadratic taper one reduces the total length of the resistive card in achieving the same scattering as that from a linear taper. The model and data provided in this report could be used in making trade-off decisions in choosing a linear versus a quadratic taper.

Diffraction coefficients based on the PO approximation were also derived and their accuracy was examined by comparison with the analytically derived coefficient and that based on a numerical model. For E-polarization it was found that the PO approximation is acceptable when the coefficient of the linear taper is less than 0.2 and in the case of quadratic tapers when the coefficient is less than 0.5.

Since the validity of PO approximation is compromised only when there is strong diffraction from the junction one may conclude that for low RCS design tapers the PO approximation should be sufficient. However, it is possible to improve upon the PO approximation by iterating on the exact integral equation in the spectral or spatial domain. We have not pursued this as yet, but it would be a worthwhile task to consider in the future.

References

[1] Roberto G. Rojas, "Wiener-Hopf analysis of the EM diffraction by an impedance discontinuity in a Planar Surface and by an Impedance Half-Plane,' *IEEE Trans. Antennas Propagat.*,vol. AP-36, No.1, pp. 71-83, 1988.

[2] Mark A. Ricoy and John L. Volakis, "Electromagnetic scattering from two-dimensional thick material junctions," University of Michigan Technical Report, 025921-14-T, 1990.

[3] Alinur Büyükaksoy, Gökhan Uzgören, and A. Hamit Serbest, "Diffraction of an obliquely incident plane wave by the discontinuity of a two part thin dielectric plane," *Int. J. Engng. Sci.*, vol. 27, no. 6, pp. 701-710, 1989.

[4] Alinur Büyükaksoy, Gökhan Uzgören, and A. Hamit Serbest, "Diffraction coefficient related to a discontinuity formed by impedance and resistive halfplanes," *IEE Proceedings*, vol. 36, Pt. H, no. 1, Feb. 1989.

[5] T.B.A. Senior, "Diffraction by a material junction," submitted to *IEEE Trans. Antennas Propagat.*, 1990.

[6] T.B.A. Senior, "Skew incidence on a material junction," *Radio Sci.*, vol. 26, no. 2, pp. 305-311, 1991.

[7] S-I Yang, J-W Ra and T.B.A. Senior, "E-polarized scattering by a resistive half plane with linearly varying resitivity," *Radio Sci.*, vol. 23, pp. 463-469, 1988.

[8] M.J. Kontorovich and N.N Lebedev, "On a method of solution of some problems of the diffraction theory," *J. Phys. USSR*, vol. 1, pp. 229-241, 1939.

[9] Milton Abramowitz and Irene Stegun, Handbook of Mathematical Functions, Dover Publications, Inc., New York, 1965.

[10] Randy L. Haupt and Valdis V. Liepa, "Synthesis of resistive tapers to control scattering patterns of strips," University of Michigan Technical Report, 024712-1-F, 1988.

[11] Gabriel F. Herrmann, "Numerical Computation of Diffraction Coefficients," *IEEE Trans. Antennas Propagat.*,vol. AP-35, No. 1, pp. 53-61, 1987.

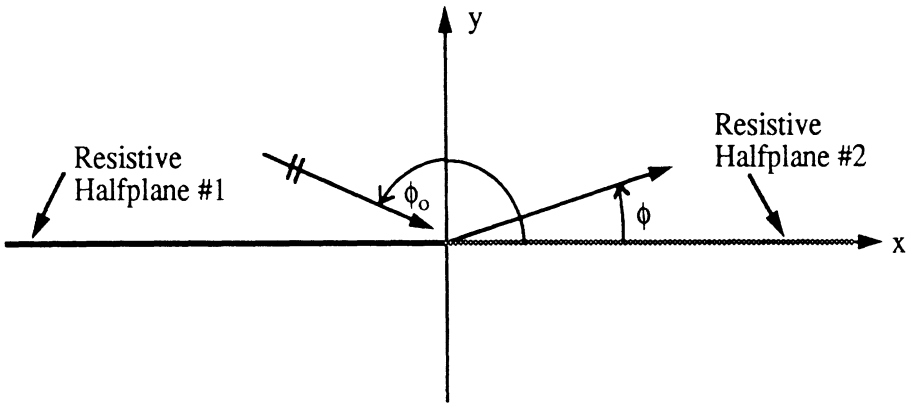

Figure 1a. Coplanar resistive halfplane geometry.

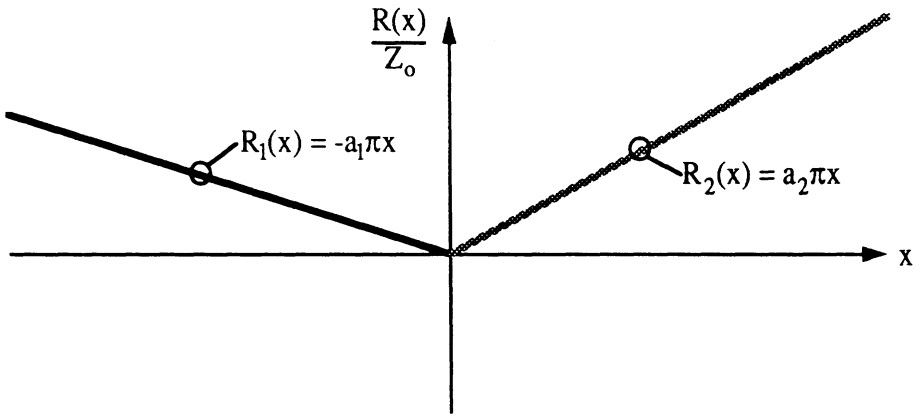

Figure 1b. Resistivity profile for two abutting linearly tapered resistive halfplanes.

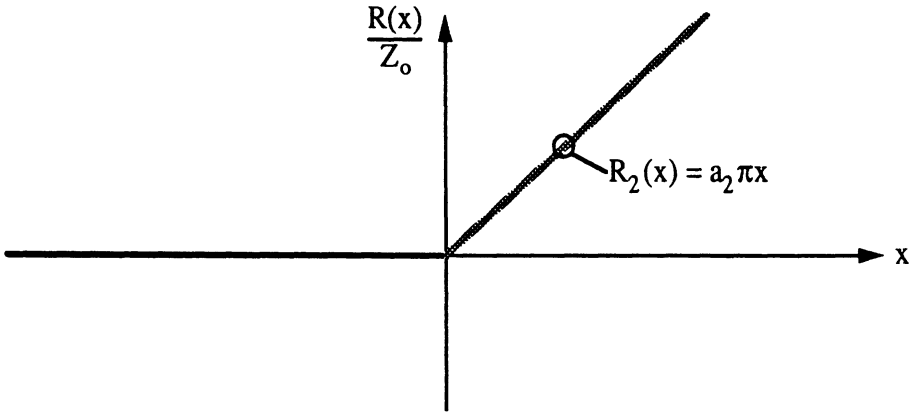

Figure 1c. Resistivity profile for a PEC halfplane linearly tapered resistive sheet junction.

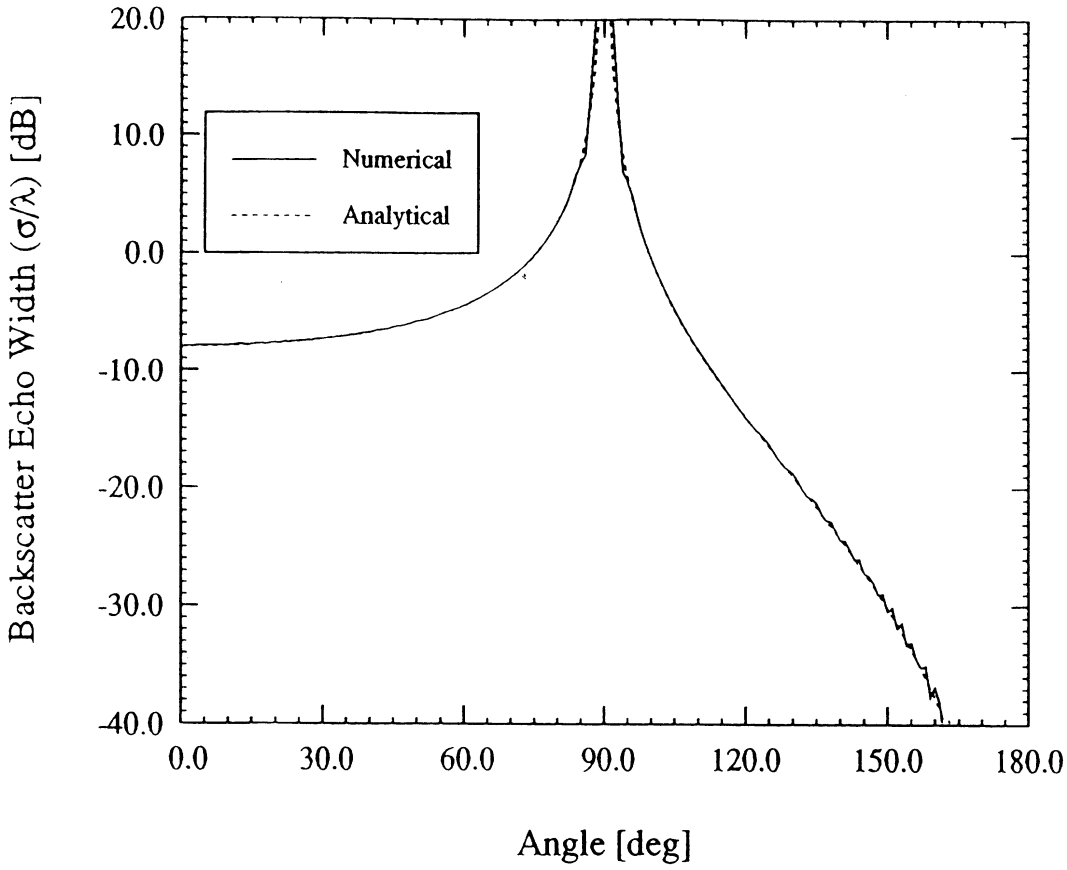

Figure 2. Comparison of the E-polarization diffraction coefficients for a PEC half plane as obtained from the numerical model and its analytical expression.

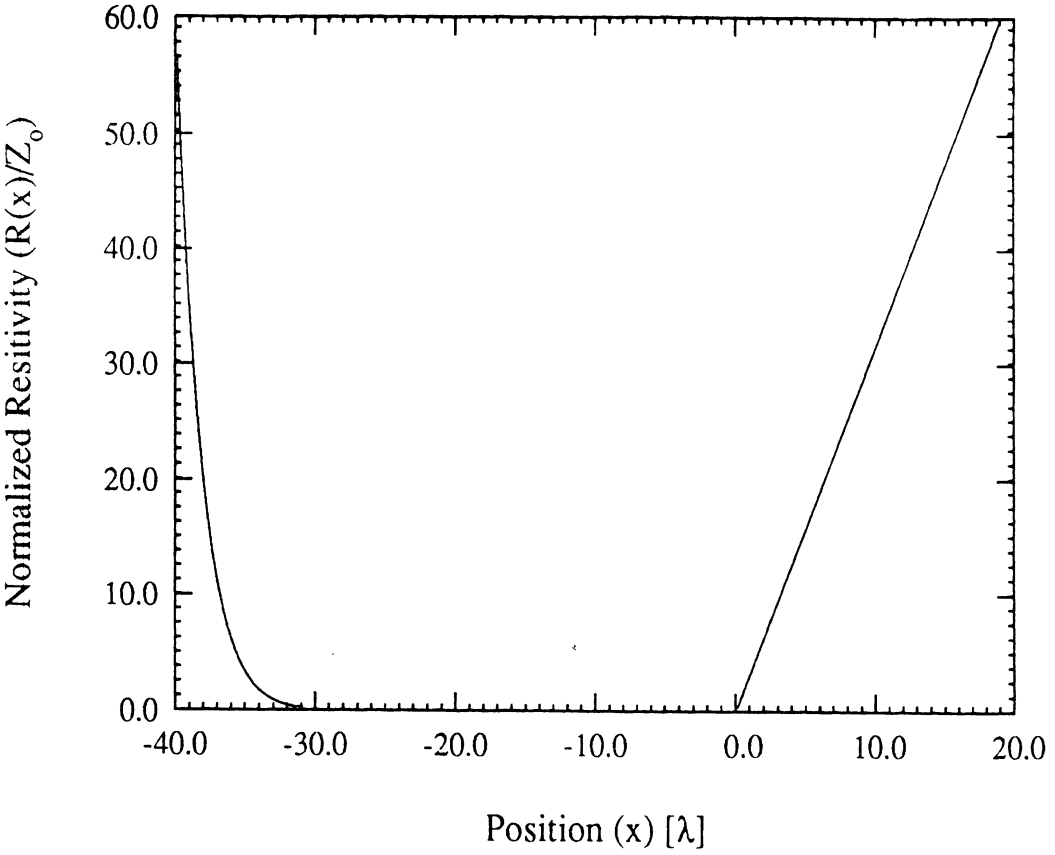

Figure 3a. Plot of the resistivity profile function given by (41) with $a_2 = 1$ and $x_{term} = 20$.

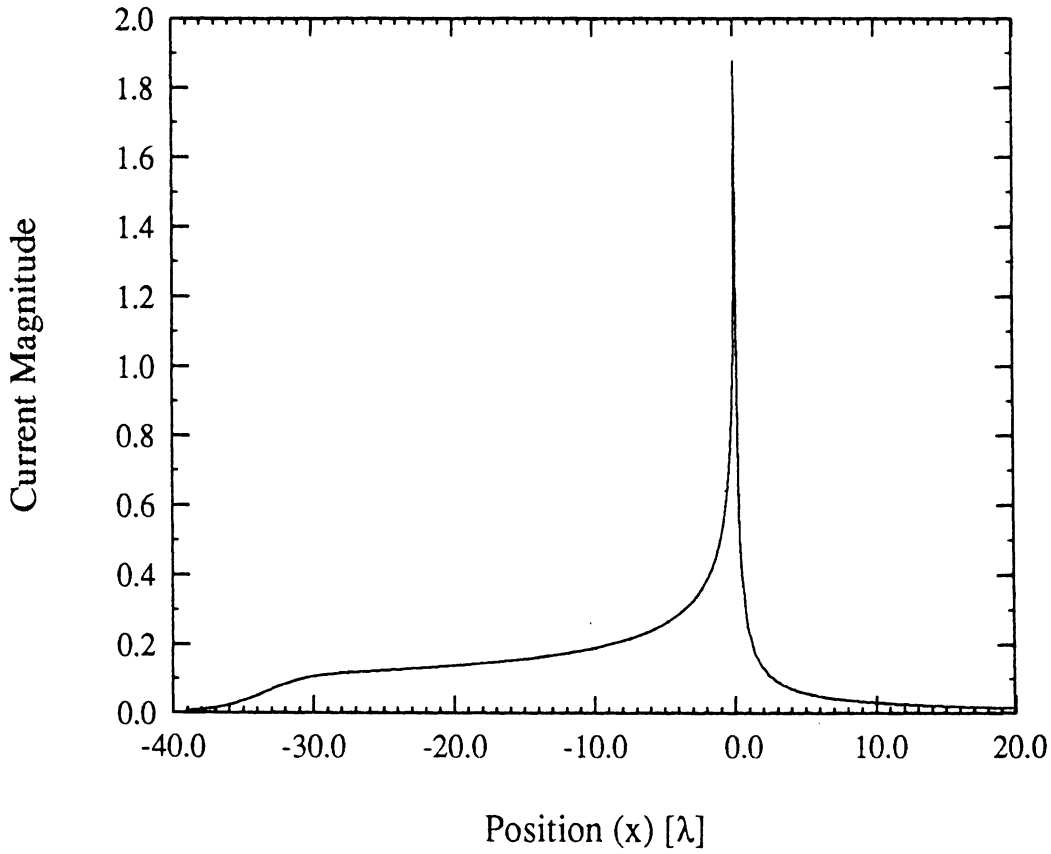

Figure 3b. Current distribution at edge-on incidence correpsonding to the resistivity profile given in figure 3a.

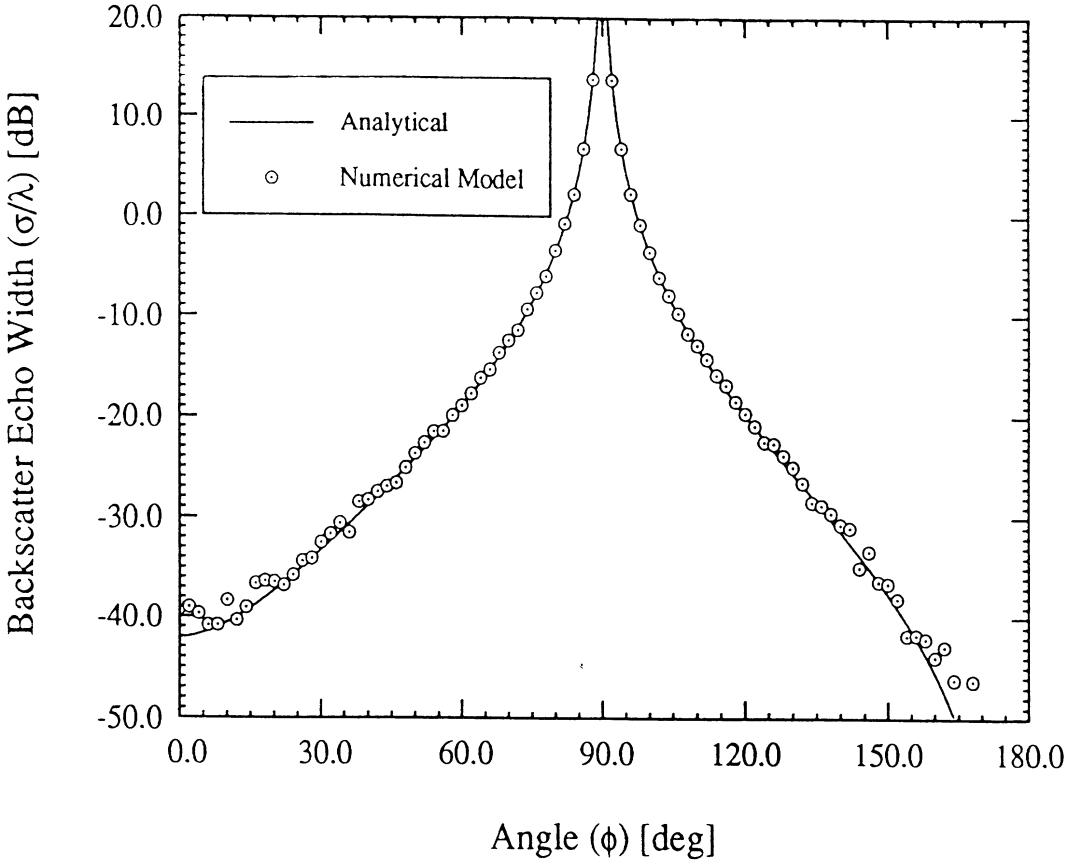

Figure 4. Comparison of the E-polarization diffraction coefficient for a_2=0.5 as computed from (39) and the numerical model.

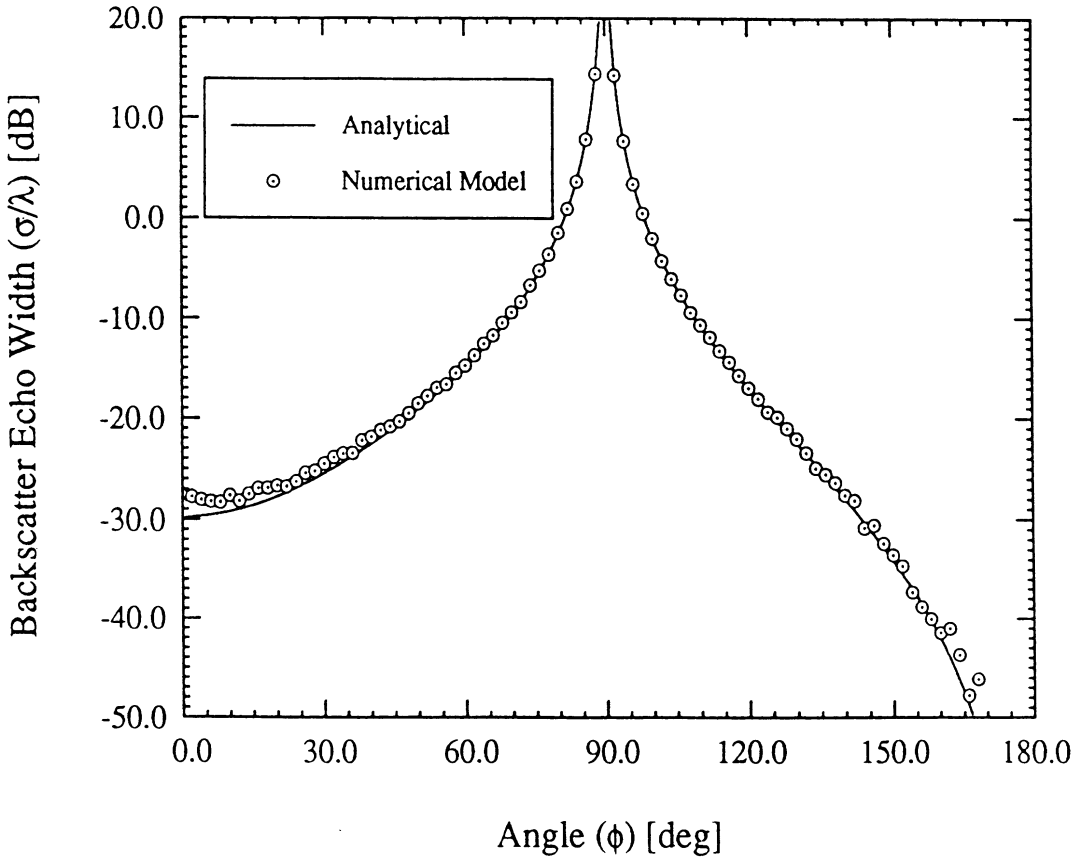

Figure 5. Comparison of the E-polarization diffraction coefficient for a_2=1 as computed from (39) and the numerical model.

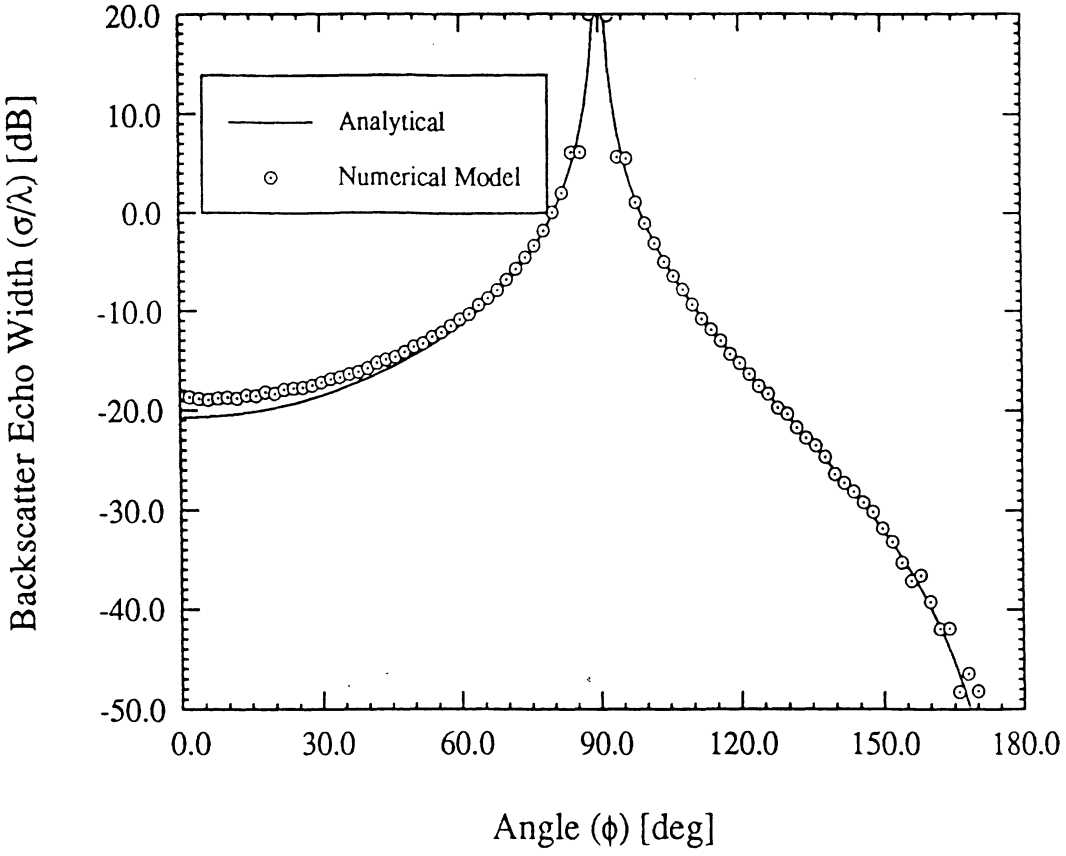

Figure 6. Comparison of the E-polarization diffraction coefficient for a_2=2 as computed from (39) and the numerical model.

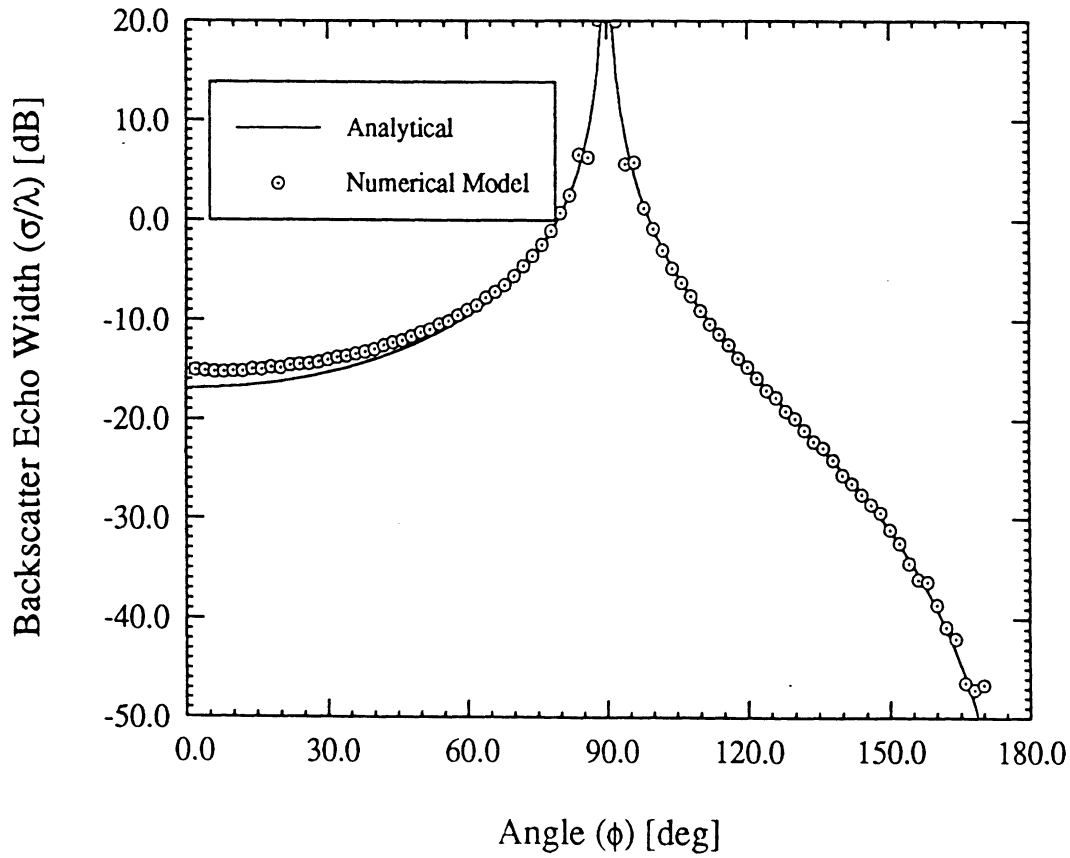

Figure 7. Comparison of the E-polarization diffraction coefficient for a_2=3 as computed from (39) and the numerical model.

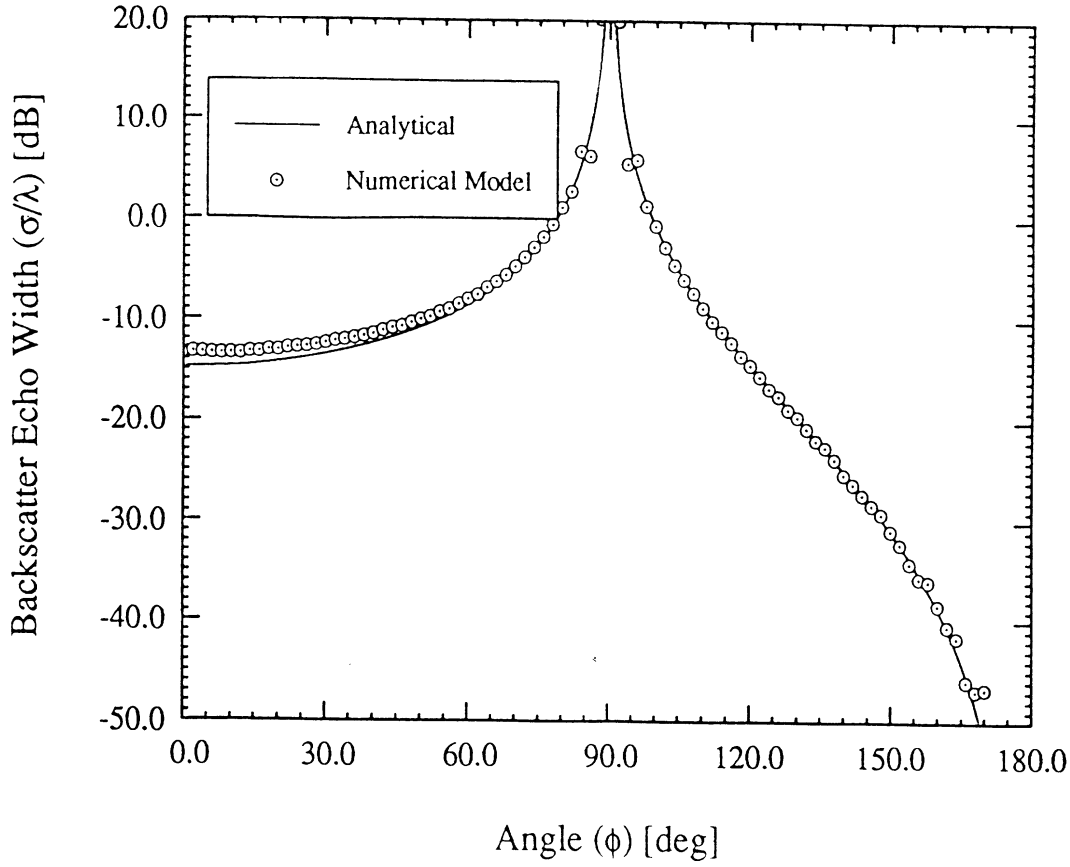

Figure 8. Comparison of the E-polarization diffraction coefficient for a_2=4 as computed from (39) and the numerical model.

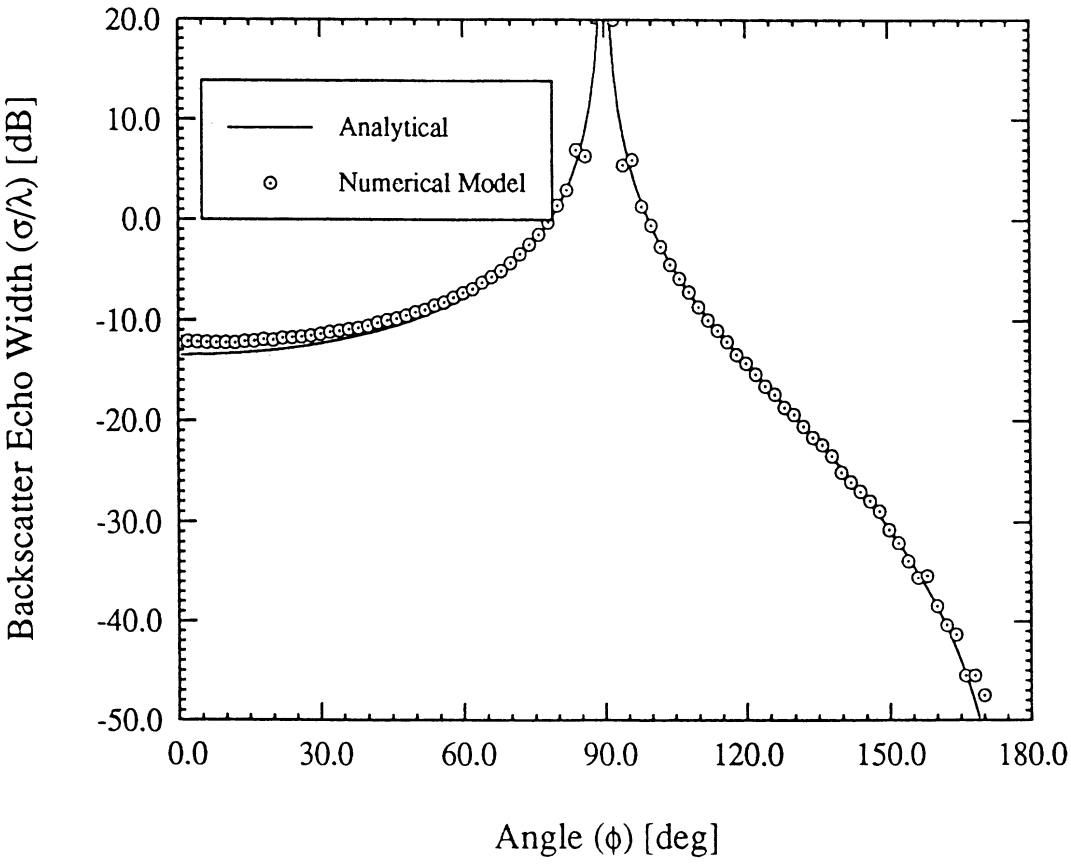

Figure 9. Comparison of the E-polarization diffraction coefficient for a_2=5 as computed from (39) and the numerical model.

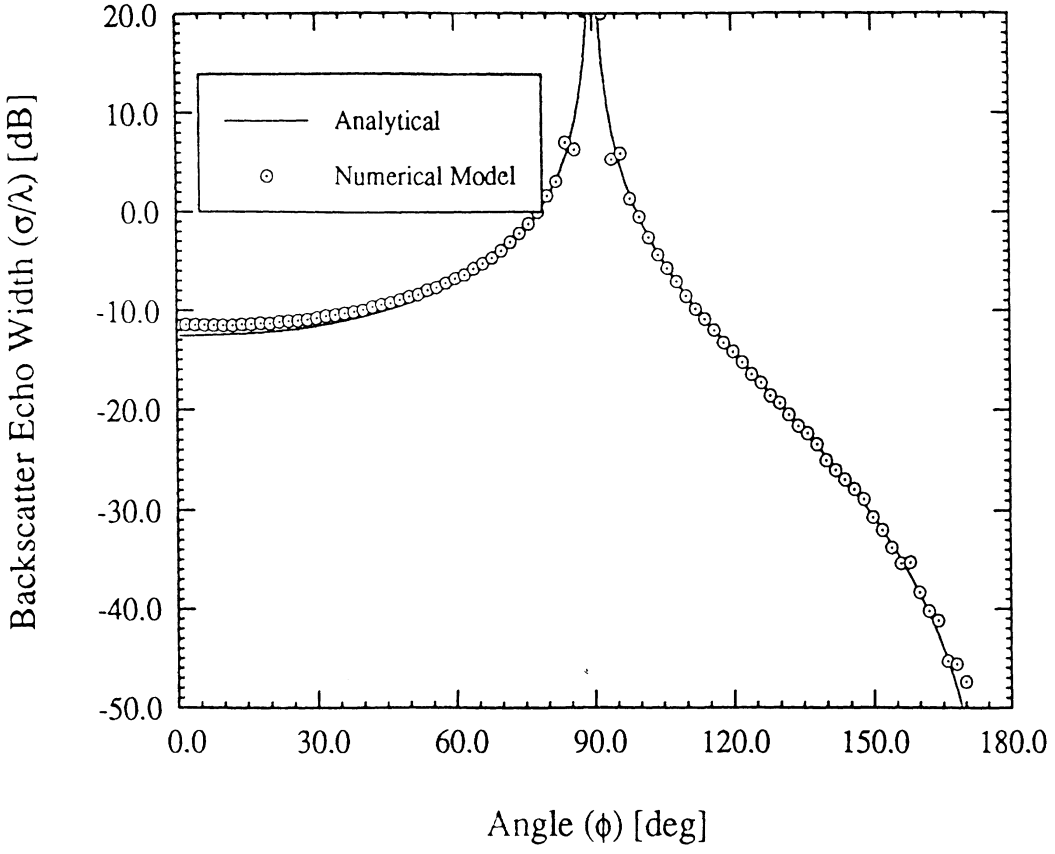

Figure 10. Comparison of the E-polarization diffraction coefficient for a_2=6 as computed from (39) and the numerical model.

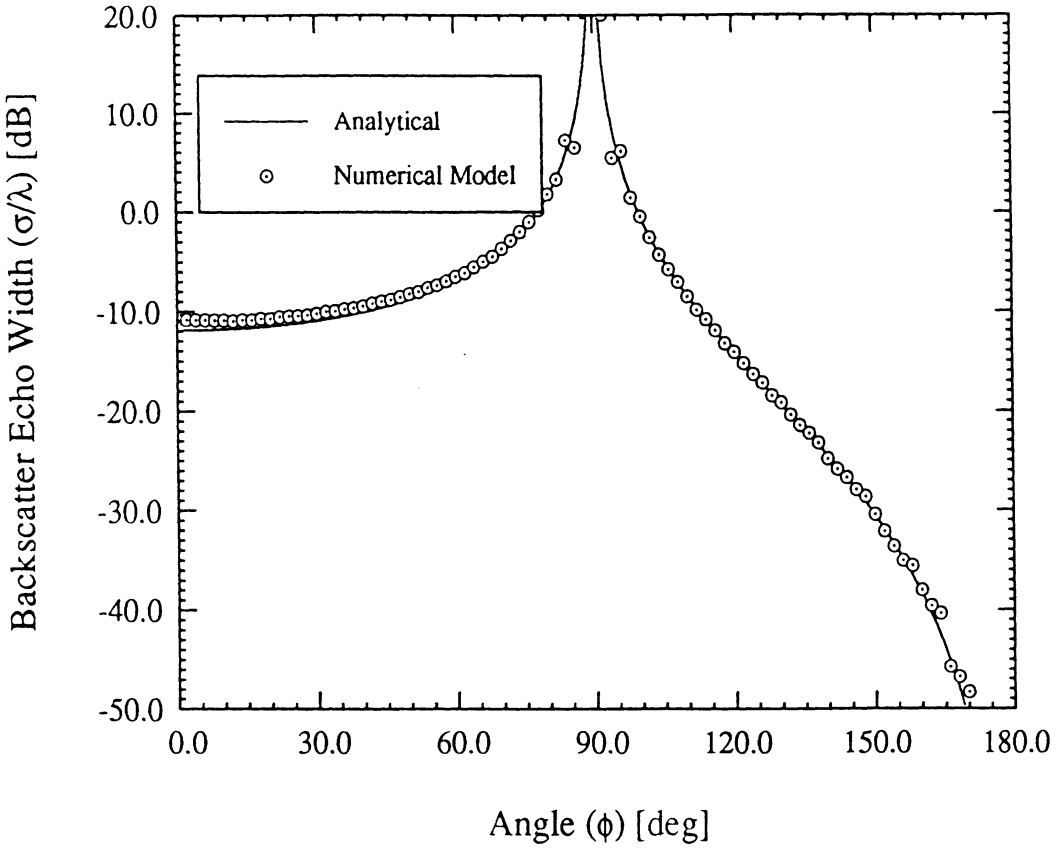

Figure 11. Comparison of the E-polarization diffraction coefficient for a_2=7 as computed from (39) and the numerical model.

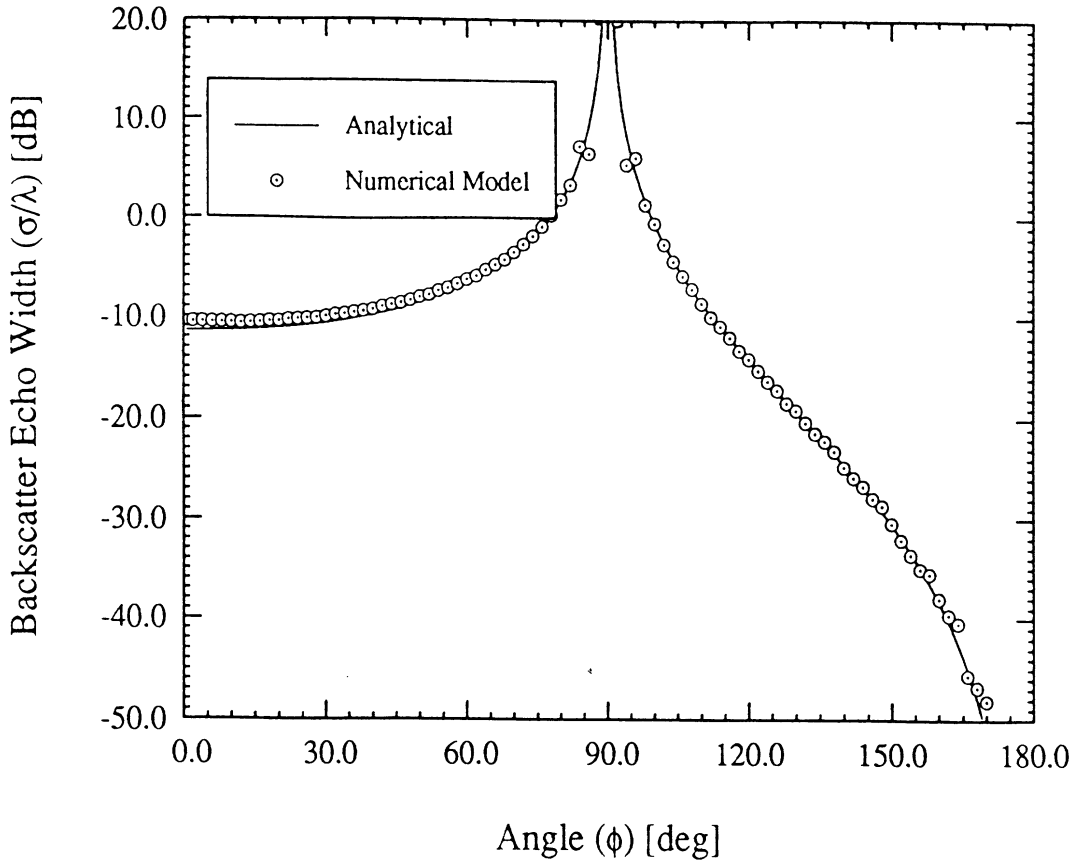

Figure 12. Comparison of the E-polarization diffraction coefficient for a_2=8 as computed from (39) and the numerical model.

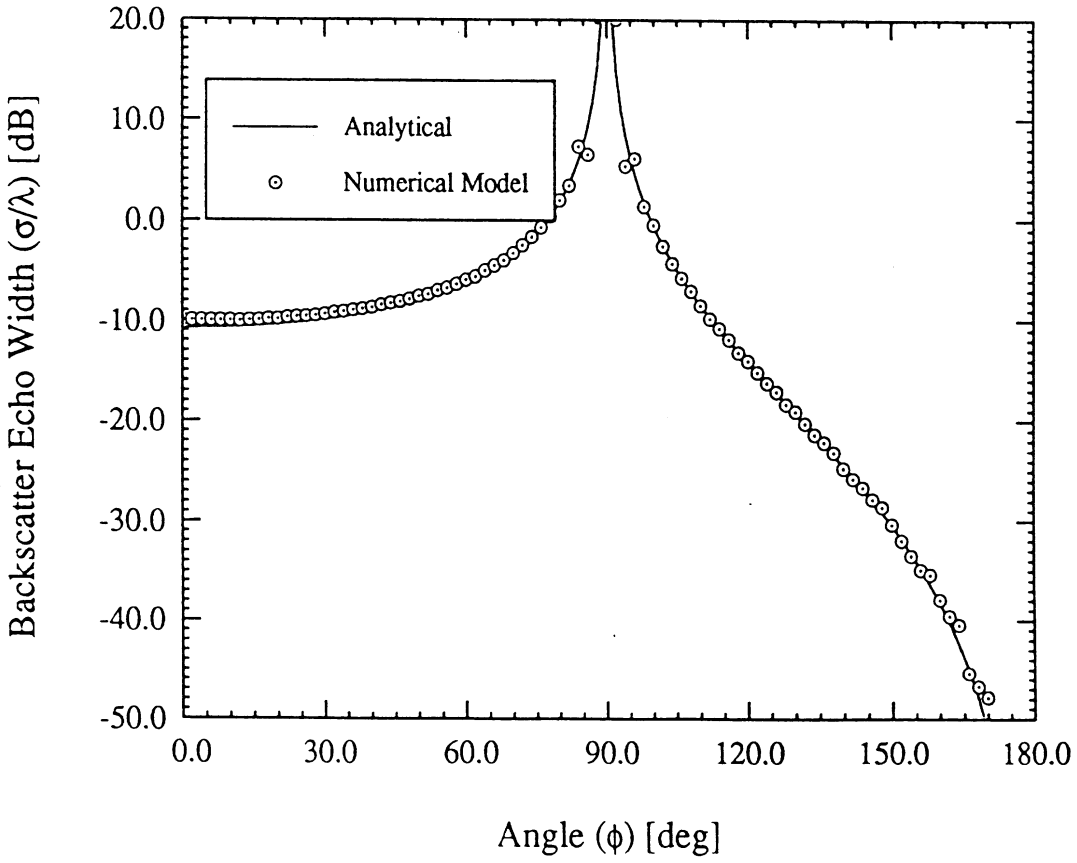

Figure 13. Comparison of the E-polarization diffraction coefficient for a_2=10 as computed from (39) and the numerical model.

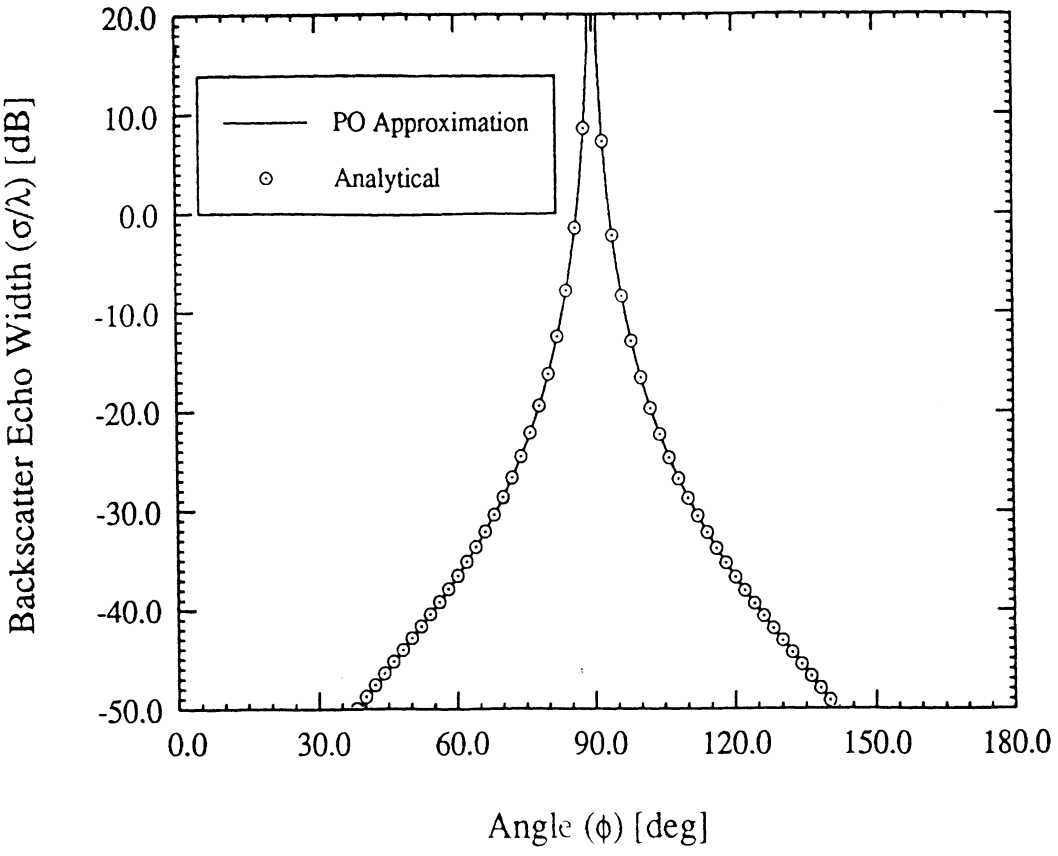

Figure 14. Comparison of the PO and numerical E-polarization backscatter echowidth for a metal-to-a linear resistive sheet junction with a_2=0.05 (see (46)).

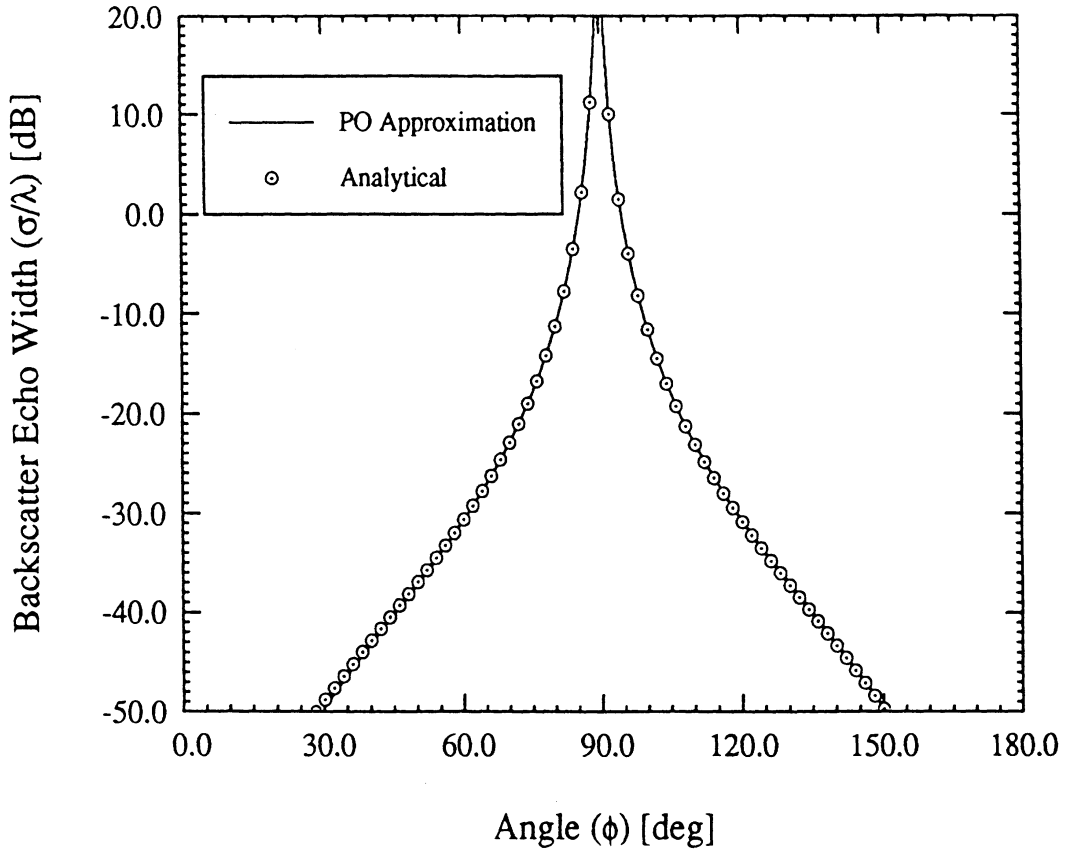

Figure 15. Comparison of the PO and numerical E-polarization backscatter echowidth for a metal-to-a linear resistive sheet junction with a_2=0.1 (see (46)).

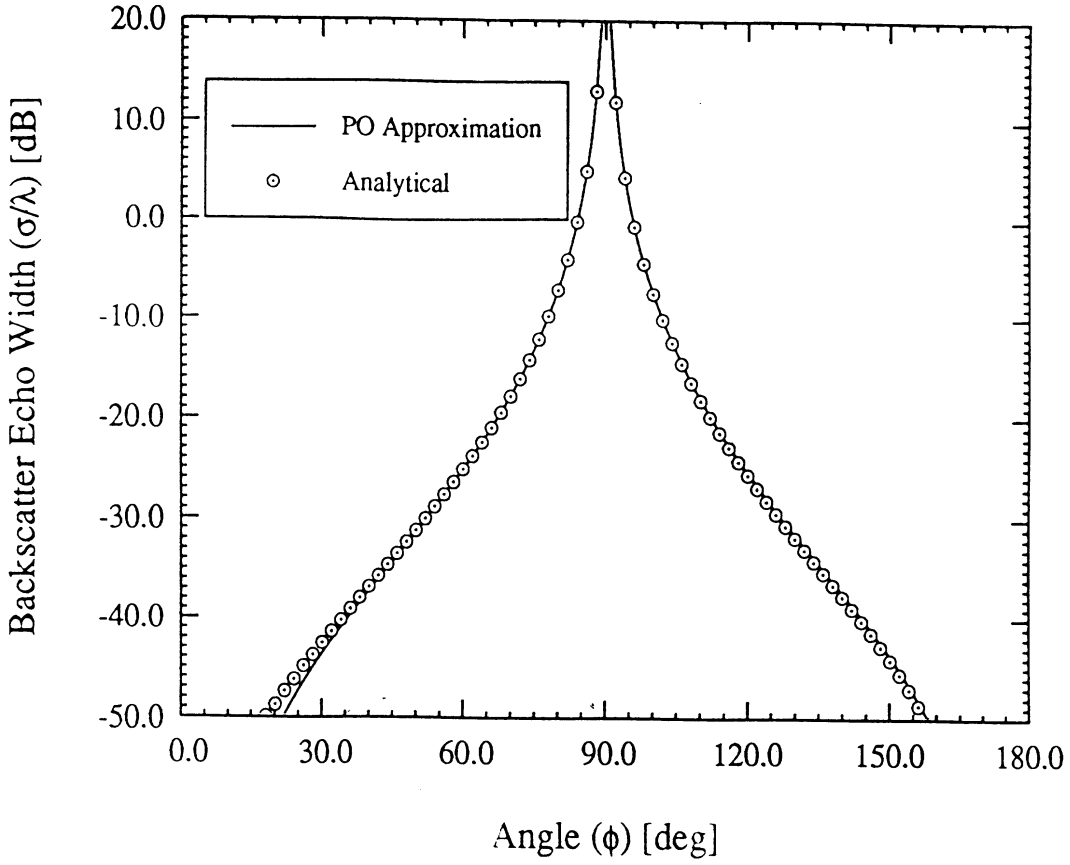

Figure 16. Comparison of the PO and numerical E-polarization backscatter echowidth for a metal-to-a linear resistive sheet junction with a_2=0.2 (see (46)).

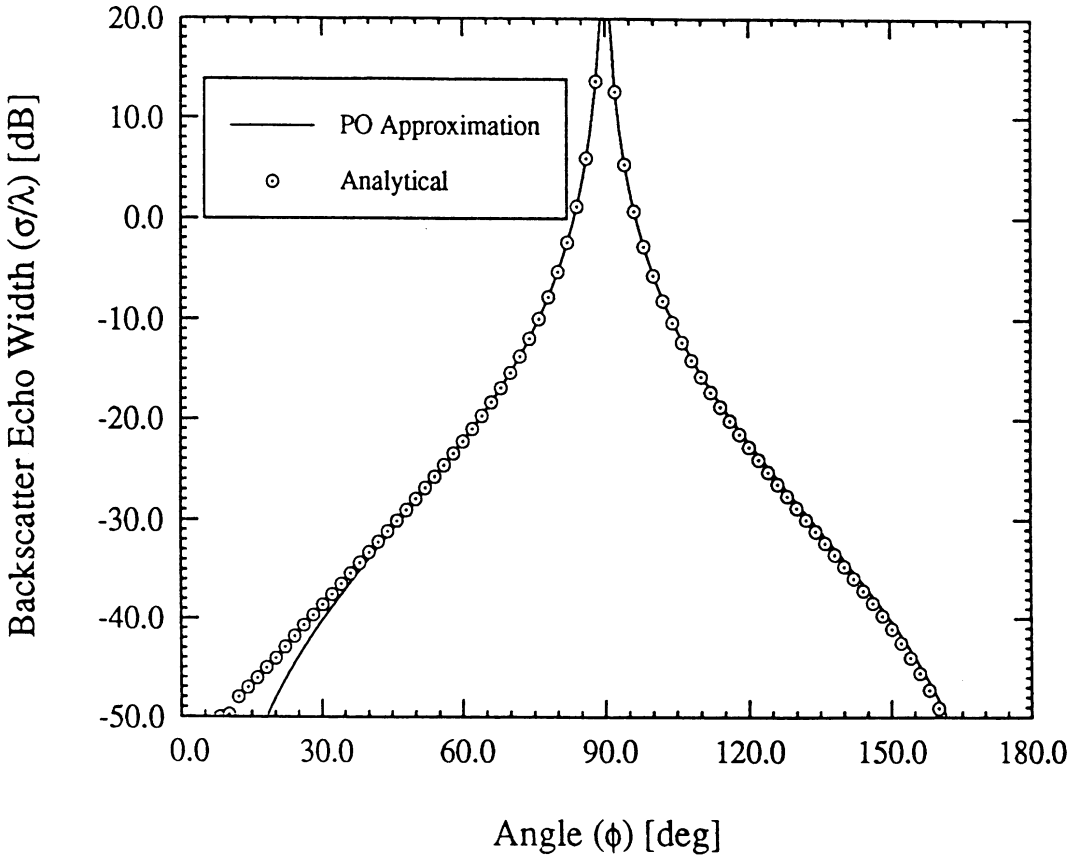

Figure 17. Comparison of the PO and numerical E-polarization backscatter echowidth for a metal-to-a linear resistive sheet junction with a_2=0.3 (see (46)).

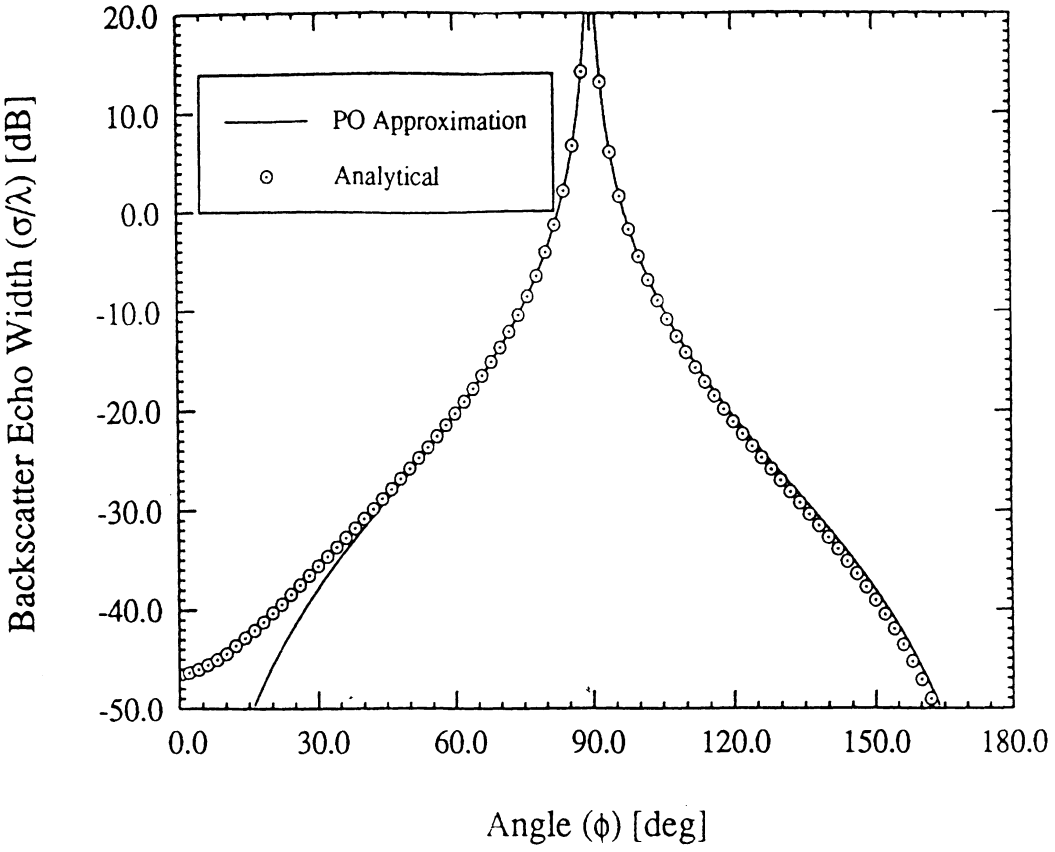

Figure 18. Comparison of the PO and numerical E-polarization backscatter echowidth for a metal-to-a linear resistive sheet junction with a_2=0.4 (see (46)).

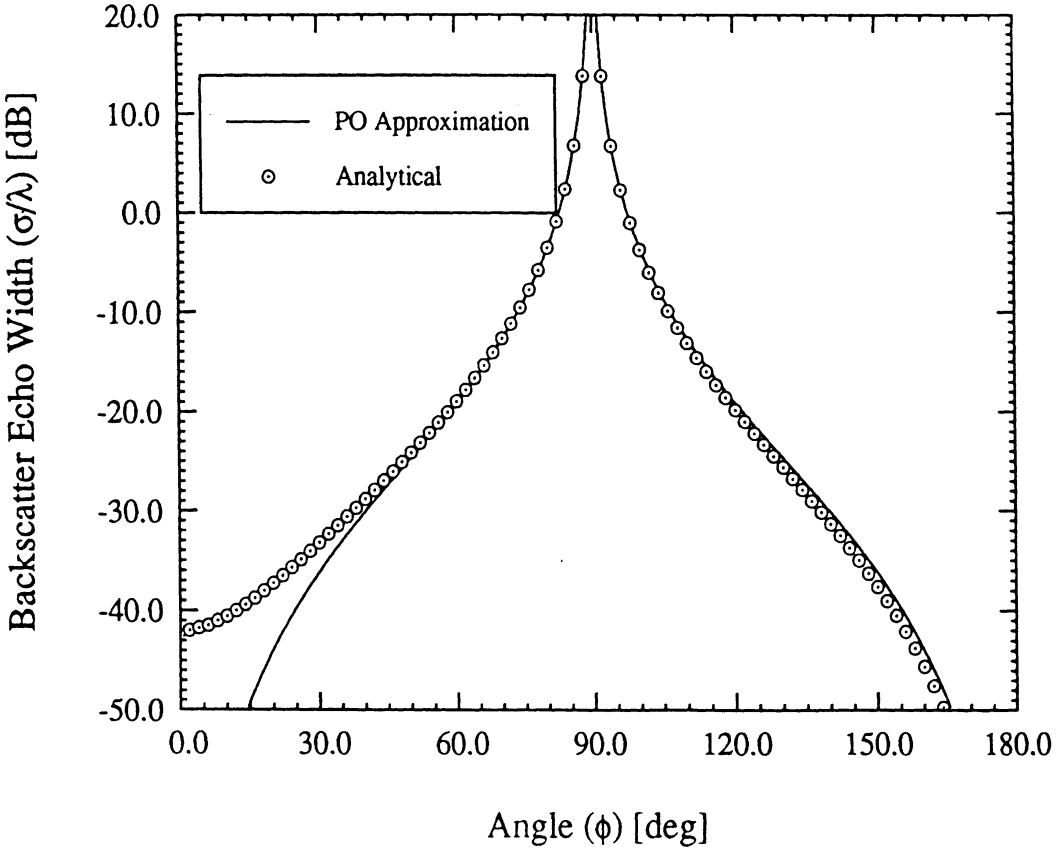

Figure 19. Comparison of the PO and numerical E-polarization backscatter echowidth for a metal-to-a linear resistive sheet junction with a_2=0.5 (see (46)).

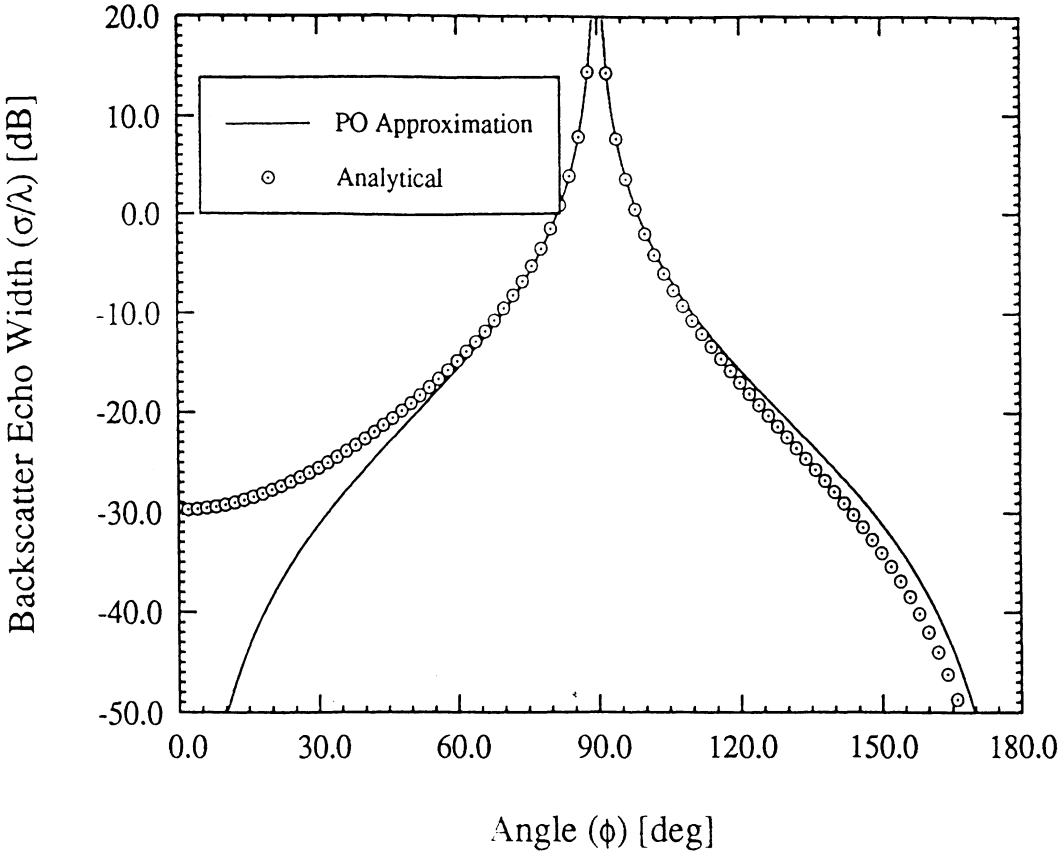

Figure 20. Comparison of the PO and numerical E-polarization backscatter echowidth for a metal-to-a linear resistive sheet junction with a_2=1 (see (46)).

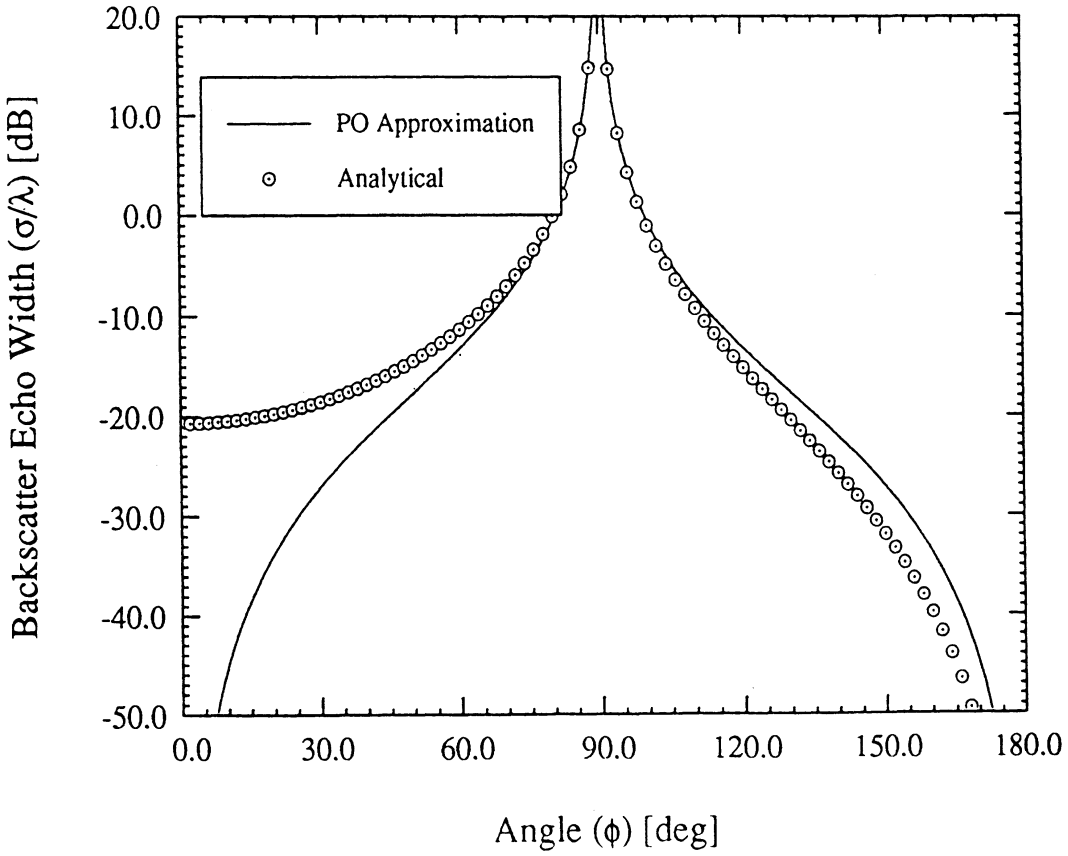

Figure 21. Comparison of the PO and numerical E-polarization backscatter echowidth for a metal-to-a linear resistive sheet junction with a_2=2 (see (46)).

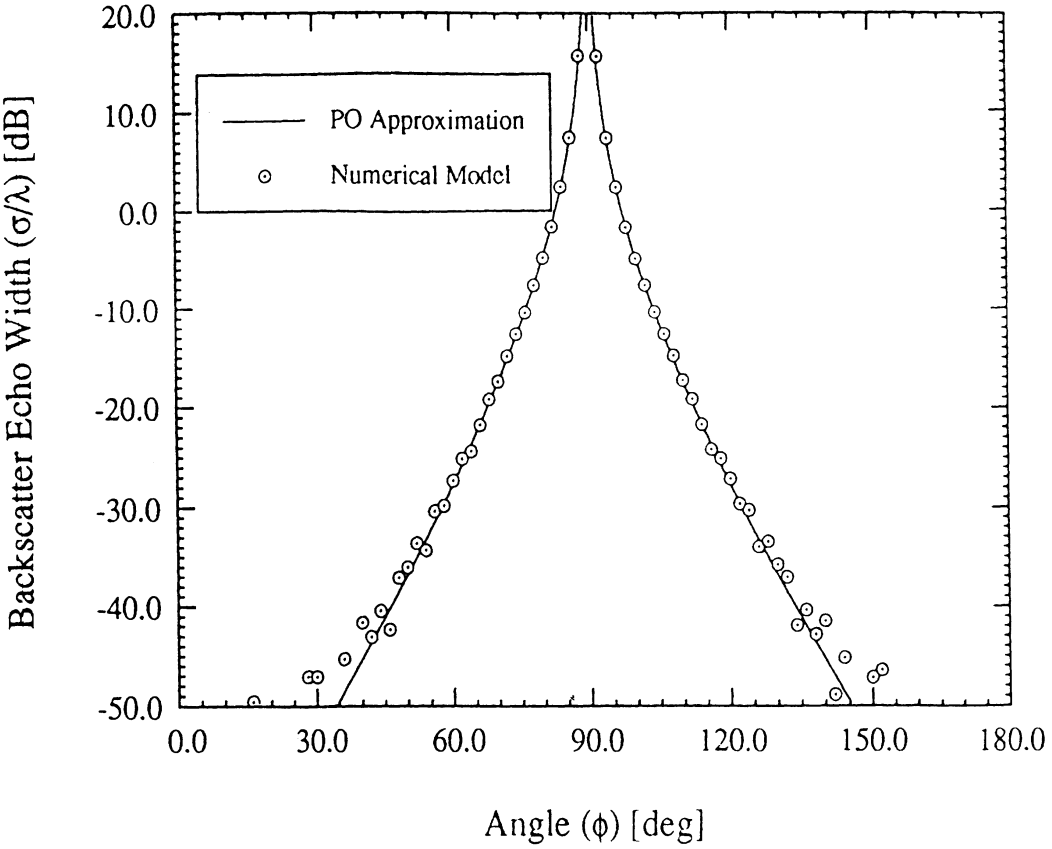

Figure 22. Comparison of the PO and numerical E-polarization backscatter echowidth from a metal-to-a quadratically tapered sheet junction having b_2=0.5 (see (50)).

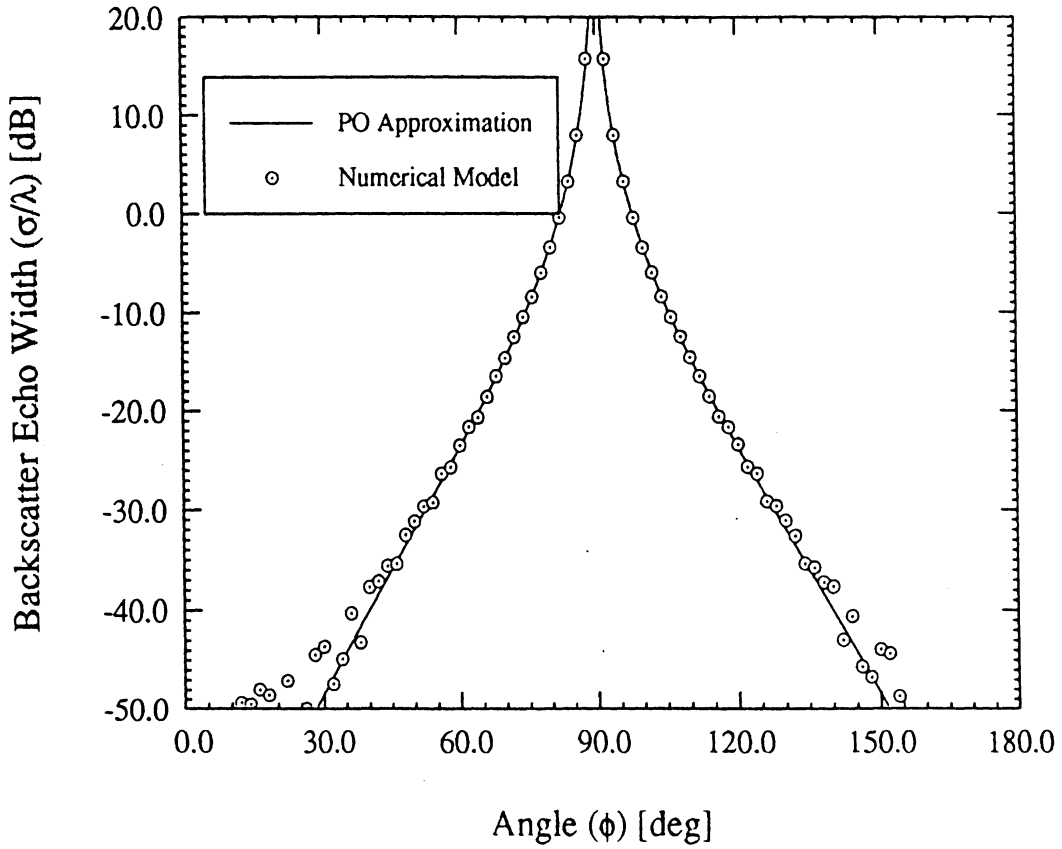

Figure 23. Comparison of the PO and numerical E-polarization backscatter echowidth from a metal-to-a quadratically tapered sheet junction having a_2=0.5 (see (50)).

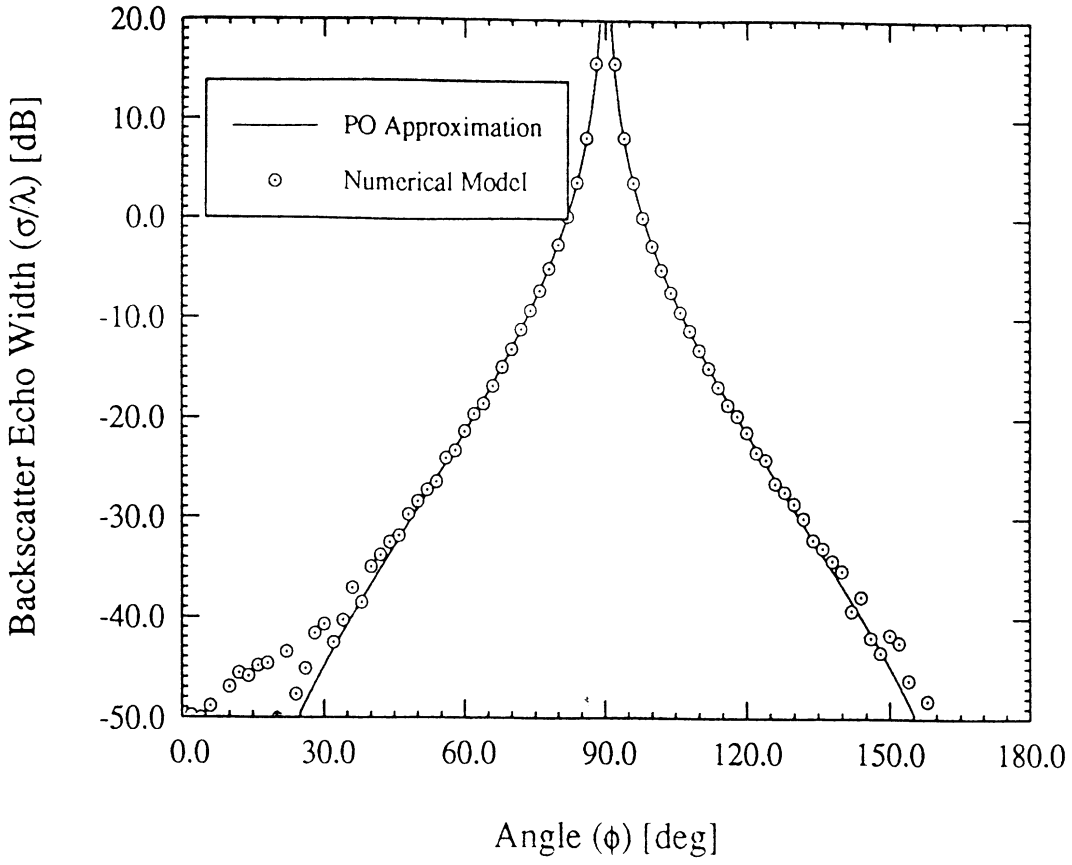

Figure 24. Comparison of the PO and numerical E-polarization backscatter echowidth from a metal-to-a quadratically tapered sheet junction having b_2=0.7 (see (50)).

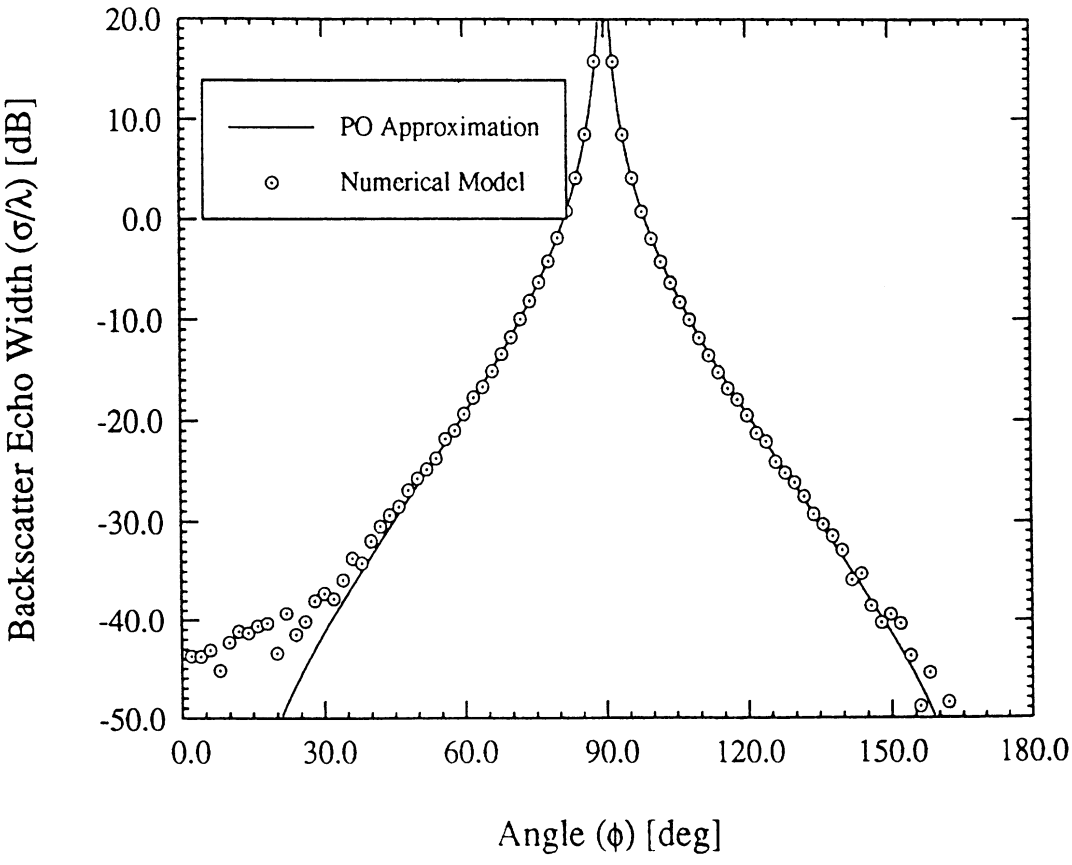

Figure 25. Comparison of the PO and numerical E-polarization backscatter echowidth from a metal-to-a quadratically tapered sheet junction having b_2=1 (see (50)).

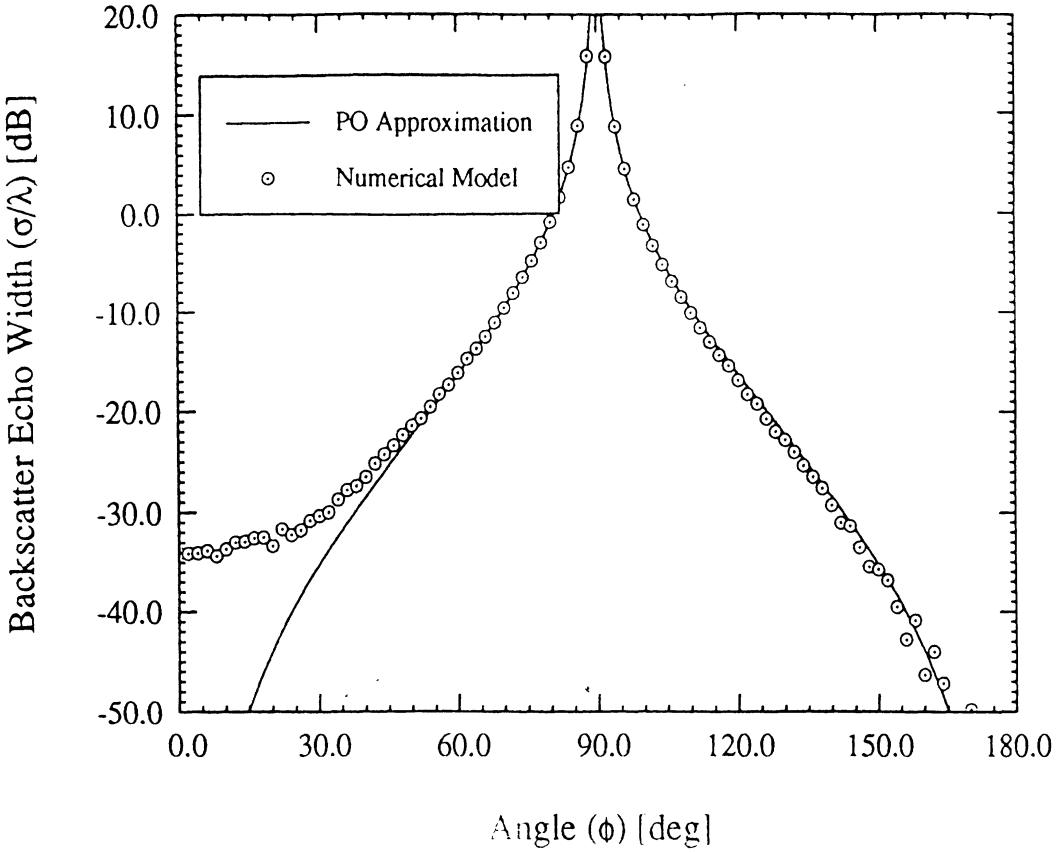

Figure 26. Comparison of the PO and numerical E-polarization backscatter echowidth from a metal-to-a quadratically tapered sheet junction having b_2=2 (see (50)).

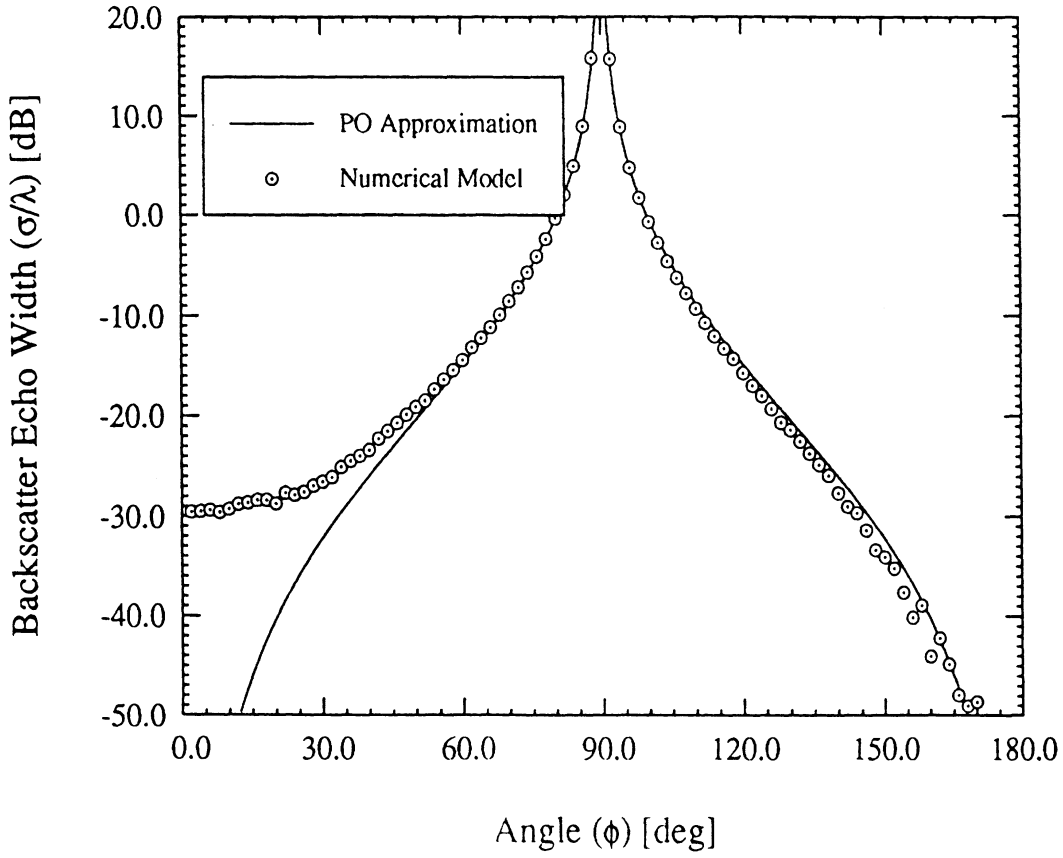

Figure 27. Comparison of the PO and numerical E-polarization backscatter echowidth from a metal-to-a quadratically tapered sheet junction having b_2=3 (see (50)).

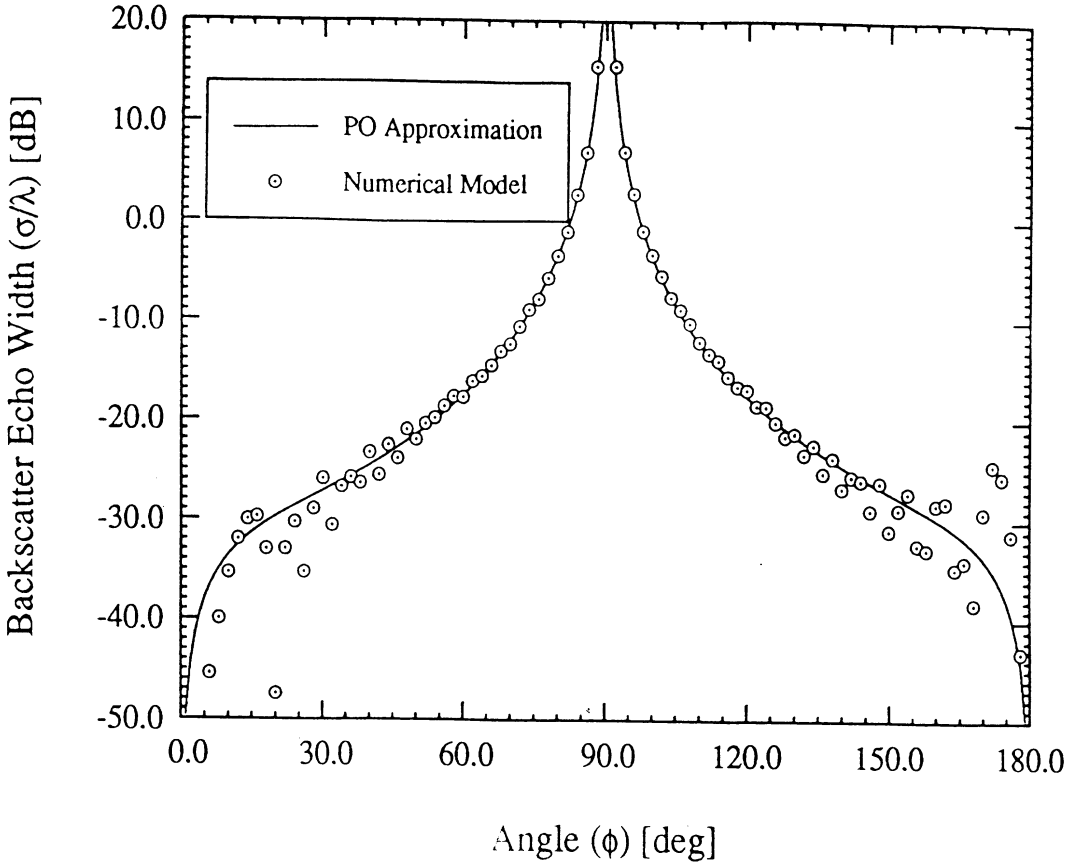

Figure 28. Comparison of the PO and numerical H-polarization backscatter echowidth for a metal-to-a linear resistive sheet junction with a_2=0.5 (see (46)).

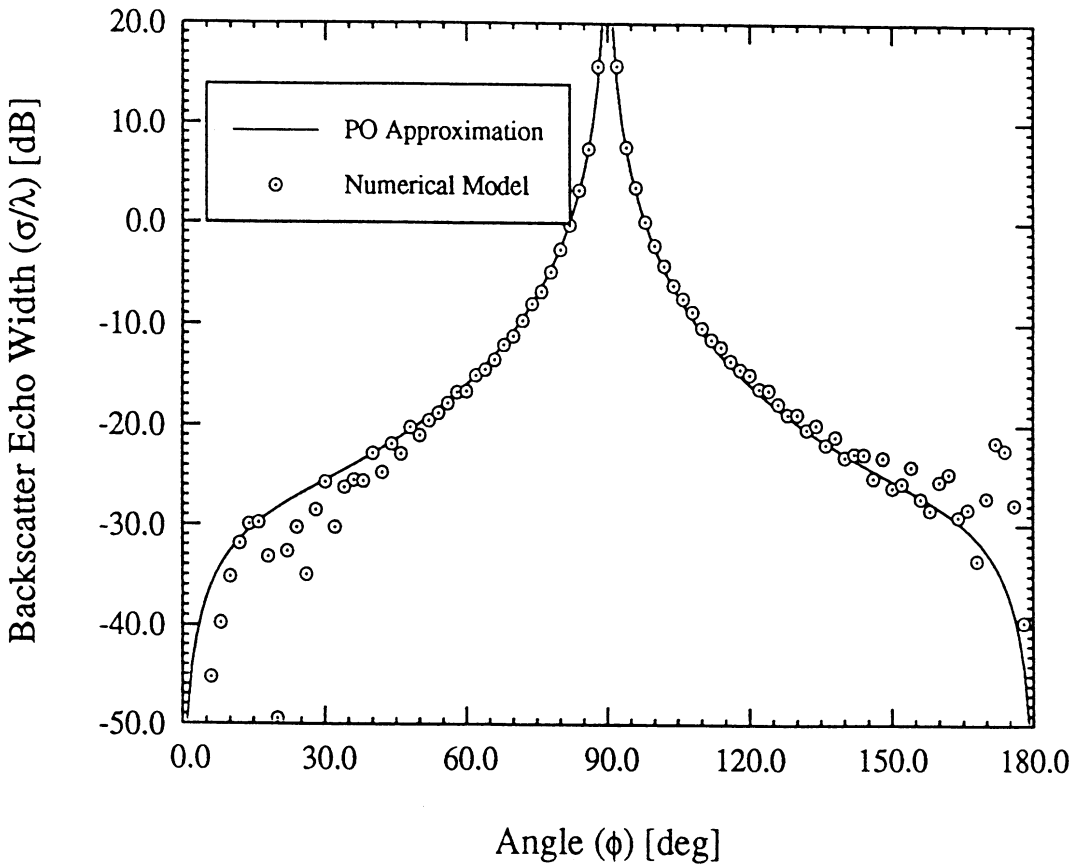

Figure 29. Comparison of the PO and numerical H-polarization backscatter echowidth for a metal-to-a linear resistive sheet junction with a_2=0.7 (see (46)).

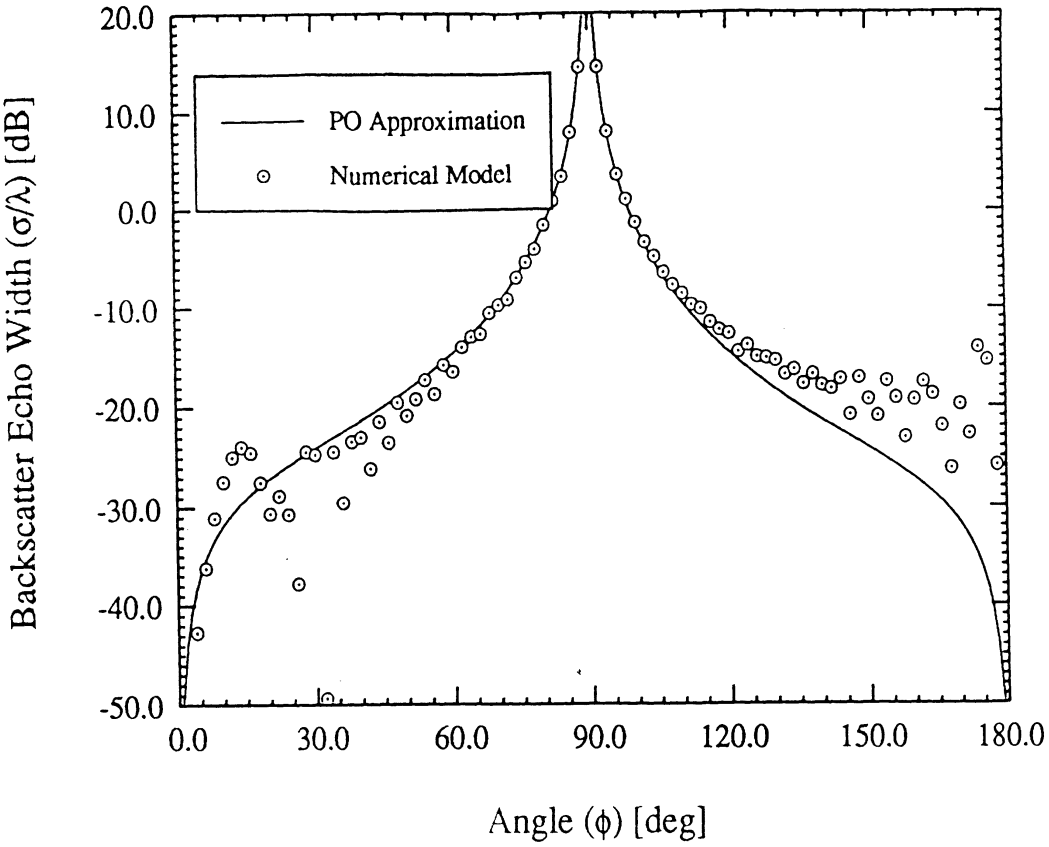

Figure 30. Comparison of the PO and numerical H-polarization backscatter echowidth for a metal-to-a linear resistive sheet junction with a_2=1 (see (46)).

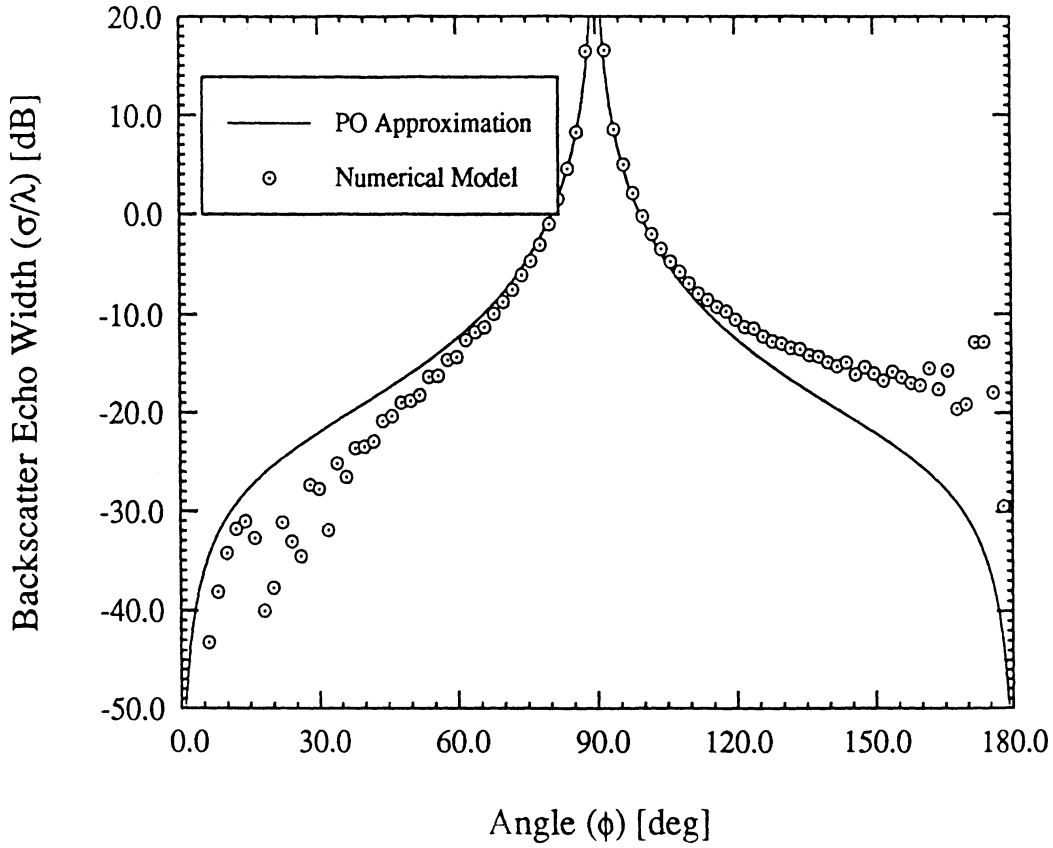

Figure 31. Comparison of the PO and numerical H-polarization backscatter echowidth for a metal-to-a linear resistive sheet junction with a_2=2 (see (46)).

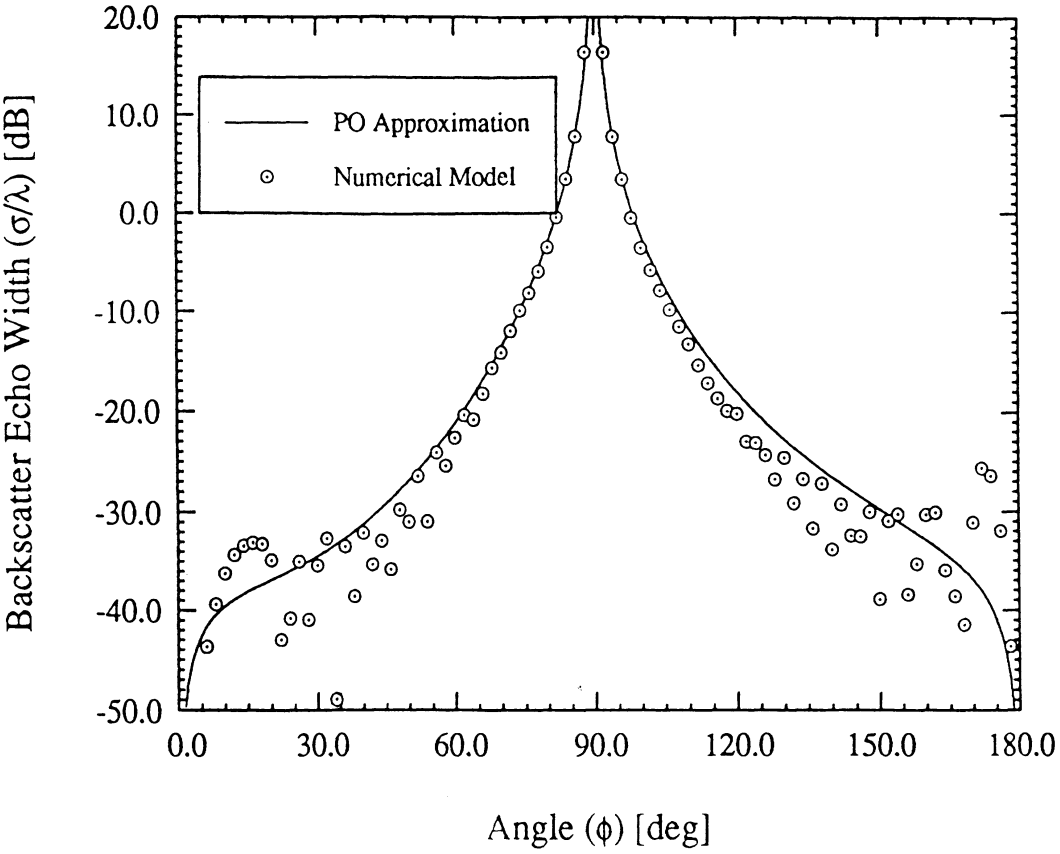

Figure 32. Comparison of the PO and numerical H-polarization backscatter echowidth from a metal-to-a quadratically tapered sheet junction having b_2=0.5 (see (50)).

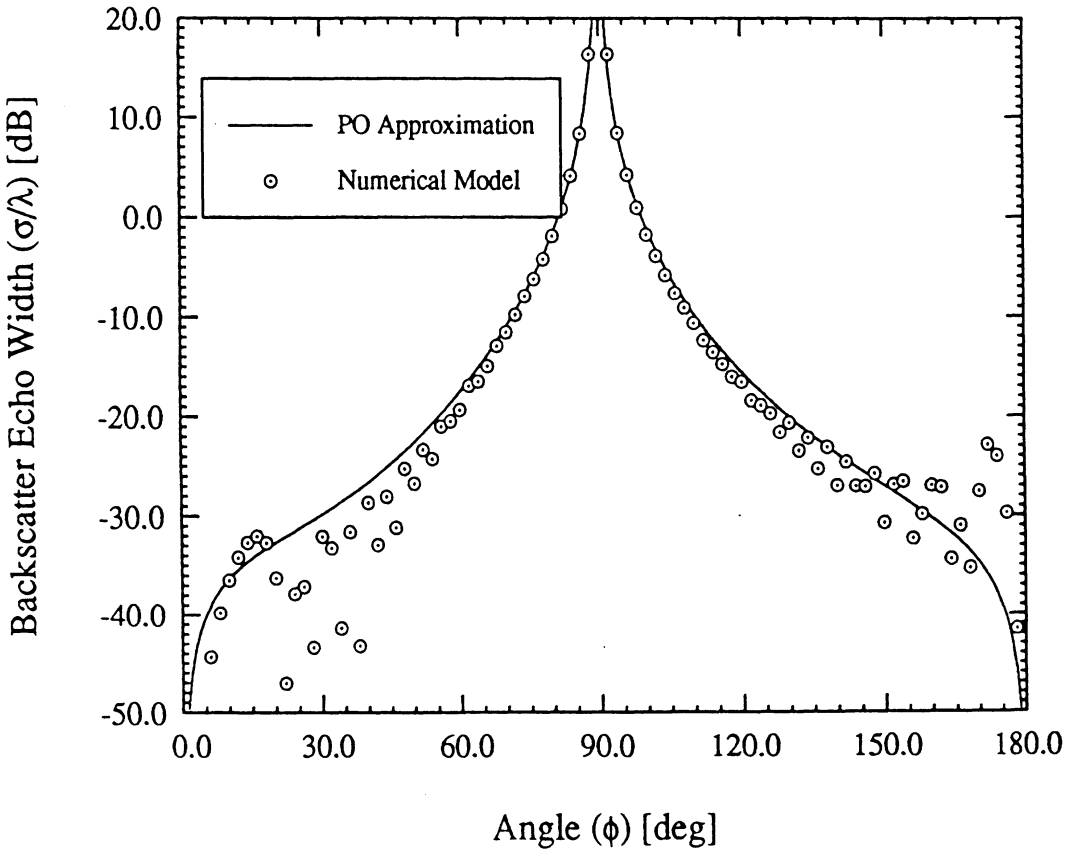

Figure 33. Comparison of the PO and numerical E-polarization backscatter echowidth from a metal-to-a quadratically tapered sheet junction having b_2=1 (see (50)).

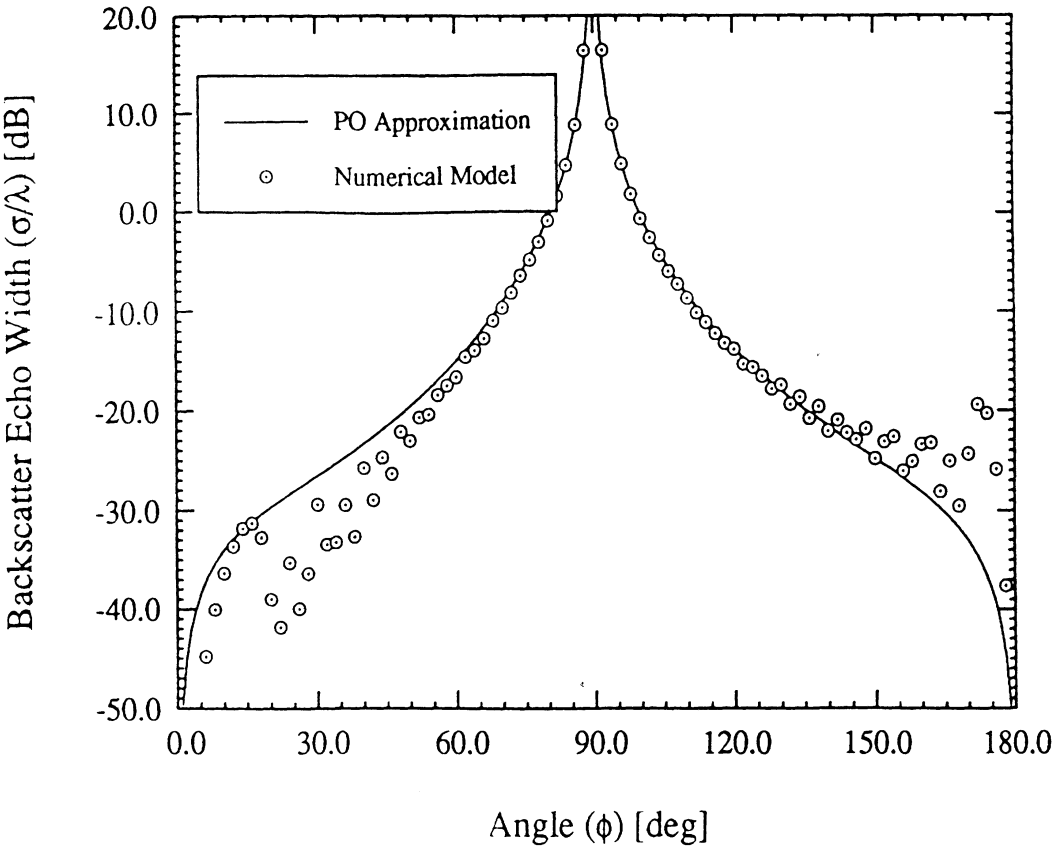

Figure 34. Comparison of the PO and numerical E-polarization backscatter echowidth from a metal-to-a quadratically tapered sheet junction having b_2=2 (see (50)).

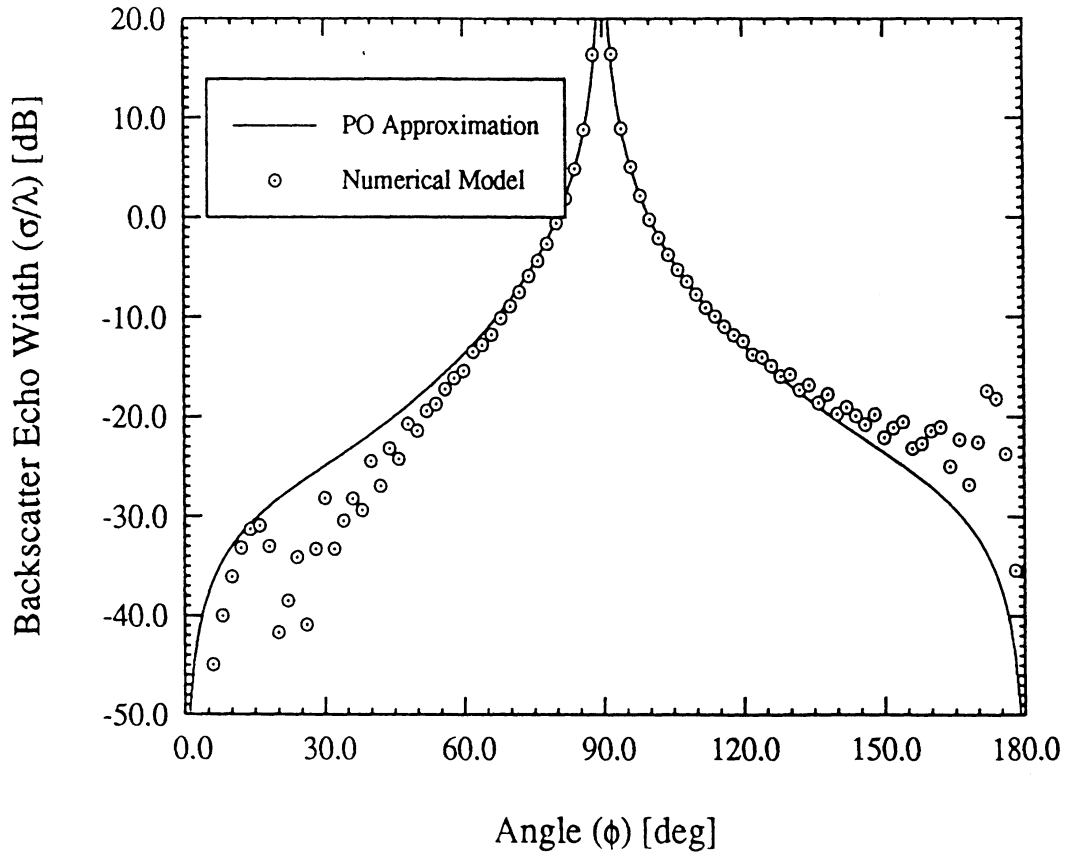

Figure 35. Comparison of the PO and numerical E-polarization backscatter echowidth from a metal-to-a quadratically tapered sheet junction having b_2=3 (see (50)).